Available online at www.sciencedirect.com
SCIENCE DIRECT®
Journal of Computational Physics 194 (2004) 742–772
JOURNAL OF COMPUTATIONAL PHYSICS
www.elsevier.com/locate/jcp

Direct simulation of particle suspensions in sliding bi-periodic frames

Wook Ryol Hwang, Martien A. Hulsen *, Han E.H. Meijer

Materials Technology, Eindhoven University of Technology, P.O. Box 513, Eindhoven 5600 MB, The Netherlands

Received 23 June 2003; received in revised form 23 September 2003; accepted 24 September 2003

Abstract

We present a new finite element scheme for direct simulations of inertialess particle suspensions in simple shear flows of a Newtonian fluid. The sliding bi-periodic domain concept of Lees and Edwards [J. Phys. C 5 (1972) 1921] has been combined with a standard velocity–pressure formulation of a fictitious-domain/finite-element method by introducing sliding bi-periodic frame constraints and it has been implemented with mortar element methods. Force-free, torque-free rigid body motions of particles are described through rigid-ring constraints and implemented by Lagrangian multipliers only on the particle boundary, which allows easy treatment of boundary-crossing particles. In our formulation, the bulk stress is obtained by simple boundary integrals of Lagrangian multipliers. Concentrating on two-dimensional circular disk particles, we discuss numerical examples of single-, two- and many-particle problems in sliding bi-periodic frames, which can represent an infinite number of such systems because of the bi-periodicity. The accuracy and convergence have been verified via comparison with a boundary-fitted mesh problem for velocities, pressures and velocity gradients. The present formulation is quite well suited for suspensions of micro/nano particles in simple shear flows and can be easily extended to viscoelastic flow problems.

Keywords: Direct numerical simulation; Particle suspensions; Lees–Edwards boundary condition; Sliding bi-periodic frame constraint; Rigid-ring description; Finite element method; Bulk stress; Suspension rheology

1. Introduction

We consider a large number of non-Brownian hard particles suspended freely in a flow where particle and fluid inertia can be neglected. We are interested in micro-structural development due to complex particle–fluid interactions in such a system, which often alters the micro-rheological properties of the fluid material, as well as bulk suspension behavior. A good example is the flow-induced crystallization phenomenon of particle-filled polymer melts during processing. The anisotropic crystallinity increases

* Corresponding author. Tel.: +31-40-247-5081; fax: +31-40-244-7355.
E-mail addresses: w.r.hwang@tue.nl (W.R. Hwang), m.a.hulsen@tue.nl (M.A. Hulsen), h.e.h.meijer@tue.nl (H.E.H. Meijer).

0021-9991/$ - see front matter
doi:10.1016/j.jcp.2003.09.023

remarkably by the presence of small rigid particles and final products then can show an outstanding impact toughness [1]. It is hypothesized that this behavior is caused by strong elongational flows between separating particles, which enhances the alignment of polymer molecules in the flow direction, accelerates the nucleation process, and finally results in additional impact strength in this direction.

In order to deal with such a problem computationally, which is a many-body and time-dependent problem in nature, one needs a direct simulation technique that gives sufficiently accurate velocity information for the fluid medium and that admits the usage of state-of-the-art viscoelastic constitutive models. Furthermore, a well-defined bi-periodic domain should be incorporated to avoid excessive computational costs, and there should not be any restriction on the particle configuration, i.e., particles should be able to cross any part of domain boundaries freely. In this way complicated wall interactions are avoided. On these length scales, it is also assumed that inertia for both particles and fluid can be neglected. In 1972 Lees and Edwards [2] proposed a bi-periodic domain concept for Molecular Dynamics simulations by describing sliding boundary conditions for simple shear flow, which is nowadays called the Lees–Edwards boundary condition (LEbc). Recently, this scheme has been used with the Lattice Boltzmann method to solve particle suspension [3] and phase separation problems [4]. It has also been applied to concentrated emulsion problems by a Lagrangian–Eulerian method with a re-meshing technique using Voronoi tessellation [5].

In the present study, we combine the LEbc with the standard velocity–pressure finite element formulation by treating the condition as kinematic constraints along the boundary in the weak form, i.e., sliding bi-periodic frame constraints. The constraint equations are implemented by Lagrangian multipliers which can be identified by traction forces on the domain boundary. To solve particle–fluid interaction problems, we employ a fictitious domain method which is similar to the distributed Lagrangian multipliers (DLM) method of Glowinski et al. [6] in that a fixed regular mesh is used for the entire computation and that hydrodynamic interaction is treated implicitly via a combined weak formulation. However, we describe a particle by its boundary only, which is filled with a fluid, the same fluid as in the fluid domain. (In two dimensions, we call it a rigid-ring description.) This description is possible because inertia is neglected. In the rigid-ring problem, we impose (unknown) rigid-body conditions only on a particle boundary and implement it by Lagrangian multipliers. The multipliers are interpreted as tractions on the particle boundary. The rigid-ring description, which requires discretization of particles only on the boundary, allows easy treatment of boundary-crossing particles. If this is the case, a particle is splitted into a few parts (maximum four) and the rigid-body motion associated with each part of the same particle can be different. A significant advantage of using two different kinds of Lagrangian multipliers, one for sliding bi-periodic constraints and the other for rigid-ring problems, is that the bulk stress, the average stress over the domain, can be expressed by simple boundary integrals of the multipliers along domain boundaries and along particle boundaries, since the multipliers are identified by boundary tractions. Moreover the integrals already exist in the global matrix system. In addition, because of discontinuous nature of the fictitious domain method, we discretize the whole domain by regular rectangular elements with bi-quadratic interpolations of the velocity and linear discontinuous interpolations of the pressure.

In the present work, we focus on simulations of circular disk particles in two-dimensional flows of a Newtonian fluid for the purpose of presenting the computational scheme and demonstrating its feasibility. However, the present scheme can be applied to three-dimensional problems without any significant modification and can easily be extended into suspension problems in viscoelastic fluids. In addition, the proposed scheme is fully implicit, thus all solutions can be obtained by solving a single matrix equation for a given particle configuration and we have no need for artificial particle collision schemes. To the authors best knowledge, this work is the first attempt to apply the LEbc to a standard velocity–pressure formulation in a finite-element method.

The paper is organized as follows: In Section 2, we give the problem definition with the governing equations for the fluid and for the particles, introducing the rigid-ring description for particles and sliding bi-periodic frame constraints for the LEbc. In Section 3, we derive weak forms for the whole domain by

modifying the original formalism of Glowinski et al. [6] to combine with rigid-ring problems and with sliding bi-periodic frame constraints, including treatments of boundary-crossing particles in the weak form. In Section 4, we discuss general expressions of the bulk stress by boundary tractions, derive identities between the tractions and the Lagrangian multipliers, and present the bulk stress expression by boundary integrals of the multipliers. In Section 5, we present implementation techniques of the weak form: discretization of the domain, point collocations for the rigid ring problem, mortar element methods with exact sliding boundary integrals for sliding bi-periodic frame constraints and time integrations. In Section 6, we verify the accuracy and convergence of our numerical scheme via comparison with a boundary-fitted mesh problem in a sliding bi-periodic frame for velocities, pressures and velocity gradients. To demonstrate the feasibility of our computational scheme, we present numerical results in Section 7 of single-, two- and many-particle problems in a sliding bi-periodic frame, which represent an infinite number of such systems. We discuss suspension rheology of disk particles in a Newtonian fluid based on the numerical results, including the effects of solid area fractions and hydrodynamic interactions.

2. Modeling

2.1. Problem definition

We consider flowing suspensions consisting of a large number of non-Brownian circular disk particles in a Newtonian fluid. Complex particle motions and hydrodynamic interactions induce complicated microstructural developments. In order to deal with such problems, a well-defined bi-periodic domain needs to be introduced, through which one can observe what happens inside. The bi-periodic domain concept may transform a suspension in an unbounded domain with an infinite number of particles into a particulate flow problem in a unit cell which can be solved at reasonable computational costs. Ideally, we want to translate the unit domain at the average velocity of the flow in a cell. In simple shear flows, the LEbc, proposed by Lees and Edwards [2] for Molecular Dynamics, satisfies the above requirements exactly, diminishing finite size effect of the computational domain. In this work, we combine the LEbc with a standard velocity–pressure formulation of finite-element methods for direct simulation of particle suspensions in simple shear flows.

Fig. 1 shows sliding bi-periodic frames and a possible particle configuration in a single frame. At an arbitrary instance, say $t = 0$, an unbounded domain of interest can be regularly divided into an infinite number of frames of the width L and the height H. As time goes on, each frame translates along the shear direction at its own average velocity (of the flow inside the frame). Rows of the frames slide relatively to one another by an amount determined by the given shear rate $\dot{\gamma}$, elapsed time t and height of the frame H. The amount of slide Δ between upper and lower frames is given by

$$\Delta = \dot{\gamma} H t. \tag{1}$$

Let us discuss a few properties of the sliding frame. First, the sliding frame is an inertial frame of reference which translates at a constant velocity. The sliding velocity of a frame is determined by the shear rate and a representative vertical position based on an arbitrary global reference coordinate. Second, the sliding frame is bi-periodic. Particles crossing the left frame boundary should re-appear on the right boundary (P_1 and P_4) and particles crossing the upper boundary should cross the lower boundary retaining their relative positions (P_2 and P_4) as shown in Fig. 1. Third, the bi-periodicity is time-dependent. Periodicity between upper and lower boundaries is determined by the amount of slide Δ which is a function of time. Thus, the location in the lower boundary, where a part of the boundary crossing particle P_2 appears, depends on elapsed time for given $(\dot{\gamma}, H)$. The same is true for the fluid particles leading to time-dependent coupling between the upper

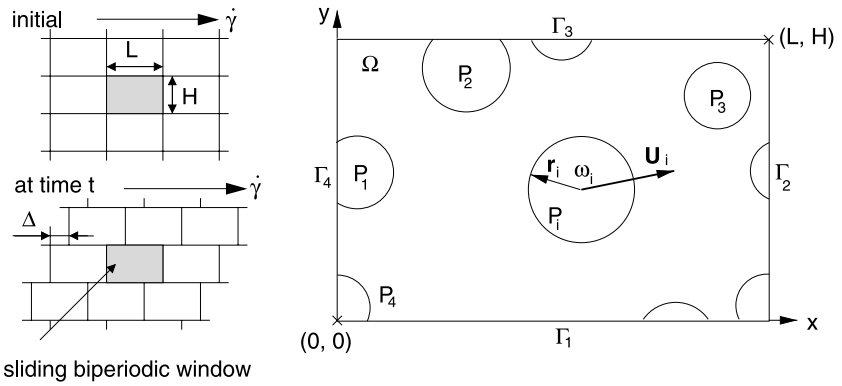

Fig. 1. Sliding bi-periodic frames in a simple shear flow (*left*). The amount of slide Δ is determined by given shear rate $\dot{\gamma}$, elapsed time t and height of the frame H. A sliding bi-periodic frame is the computational domain and a possible particle configuration inside the domain is indicated (*right*).

and lower boundaries. (Detailed mathematical descriptions of the sliding bi-periodicity will be discussed in Section 2.3.)

A sliding bi-periodic frame, denoted by Ω, is the computational domain of this work and the four boundaries of the frame are denoted by Γ_i $(i = 1\text{–}4)$ (Fig. 1). We use a symbol Γ for $\bigcup_{i=1}^{4} \Gamma_i$. The Cartesian x and y coordinates are selected as parallel and normal to the shear flow direction, respectively. Particles are denoted by $P_i(t)$ $(i = 1, \ldots, N)$ and N is the number of particles in a single frame. We use a symbol $P(t)$ for $\bigcup_{i=1}^{N} P_i(t)$, a collective region occupied by particles at a certain time t. For a particle P_i, $\boldsymbol{X}_i = (X_i, Y_i)$, $\boldsymbol{U}_i = (U_i, V_i)$, $\boldsymbol{\omega}_i = \omega_i \boldsymbol{k}$ and $\boldsymbol{\Theta}_i = \Theta_i \boldsymbol{k}$ are used for the coordinates of the particle center, the translational velocity, the angular velocity and the angular rotation, respectively; and $\boldsymbol{k}$ is the unit vector in the direction normal to the plane.

2.2. Governing sets of equations

Here, we present the governing equations in a strong form for suspensions of two-dimensional disk-like circular particles in a Newtonian fluid, neglecting inertia for both fluid and particles. For simplicity, the equations for systems consisting of only non-boundary-crossing particles are presented first. The extension to boundary-crossing particles will be treated in Section 2.4.

2.2.1. Fluid domain

The set of equations for the fluid domain is given by:

$$\nabla \cdot \boldsymbol{\sigma} = 0 \quad \text{in } \Omega \setminus P(t), \tag{2}$$

$$\nabla \cdot \boldsymbol{u} = 0 \quad \text{in } \Omega \setminus P(t), \tag{3}$$

$$\boldsymbol{\sigma} = -p\boldsymbol{I} + 2\eta \boldsymbol{D} \quad \text{in } \Omega \setminus P(t), \tag{4}$$

$$\boldsymbol{u} = \boldsymbol{U}_i + \boldsymbol{\omega}_i \times (\boldsymbol{x} - \boldsymbol{X}_i) \quad \text{on } \partial P_i(t) \qquad (i = 1, \ldots, N). \tag{5}$$

Eqs. (2)–(5) are equations for the momentum balance, the continuity, the constitutive relation, and rigid-body conditions on particle boundaries, respectively. $\boldsymbol{u}$, $\boldsymbol{\sigma}$, p, $\boldsymbol{I}$, $\boldsymbol{D}$ and η are the velocity, the stress, the

pressure, the identity tensor, the rate of deformation tensor and the viscosity, respectively. Unknown rigid-body motions in Eq. (5) will be determined by hydrodynamic interactions. In the absence of inertia, initial conditions are not necessary for the velocity of the fluid as well as the particles. In addition, there is no explicit boundary condition on the domain boundary Γ. Instead, we will introduce constraint equations on Γ in Section 2.3 to assign a simple shear flow condition, attaining bi-periodicity of the sliding frame.

2.2.2. Particle domain: rigid-ring problem

For the description of a particle in combination with fictitious domain methods, one can assign direct rigid-body motions on the region occupied by the particle [6,8], or impose zero rate-of-deformation over the region [7]. Both methods need domain discretization. In our study, we introduce an alternative description for the particle domain. We consider a circular particle as a rigid ring, which is filled with the same fluid as in the fluid domain so that the rigid-body condition is imposed on the particle boundary only. We call it the rigid-ring description. This description is possible when inertia is negligible. The rigid-ring description needs discretization only along the particle boundaries so that it gives significant reduction on memory and it is easier to implement compared with methods using domain discretization. In addition, the boundary discretization allows the systematic treatment of boundary-crossing particles, which is important in bi-periodic simulations. From the rigid-ring description, the governing equations for a region occupied by a particle P_i at a certain time t can be written as:

$$\nabla \cdot \boldsymbol{\sigma} = 0 \quad \text{in } P_i(t), \tag{6}$$

$$\nabla \cdot \boldsymbol{u} = 0 \quad \text{in } P_i(t), \tag{7}$$

$$\boldsymbol{\sigma} = -p\boldsymbol{I} + 2\eta \boldsymbol{D} \quad \text{in } P_i(t), \tag{8}$$

$$\boldsymbol{u} = \boldsymbol{U}_i + \boldsymbol{\omega}_i \times (\boldsymbol{x} - \boldsymbol{X}_i) \quad \text{on } \partial P_i(t). \tag{9}$$

Eqs. (6)–(9) are the equations for the momentum balance, the continuity, the constitutive relation and the boundary condition, respectively, which are exactly the same as fluid domain equations in Eqs. (2)–(5). The trivial solution of this problem inside a particle is simply the rigid-body motion itself, applied on the particle boundary:

$$\boldsymbol{u} = \boldsymbol{U}_i + \boldsymbol{\omega}_i \times (\boldsymbol{x} - \boldsymbol{X}_i) \quad \text{in } P_i(t). \tag{10}$$

Thus, the rigid-ring problem is a physically well-defined description for rigid particles (and can be applied to viscoelastic constitutive equations in the same way). In addition, the movement of the particles is given by the kinematic equations:

$$\frac{\mathrm{d}\boldsymbol{X}_i}{\mathrm{d}t} = \boldsymbol{U}_i, \quad \boldsymbol{X}_i|_{t=0} = \boldsymbol{X}_{i,0}, \tag{11}$$

$$\frac{\mathrm{d}\boldsymbol{\Theta}_i}{\mathrm{d}t} = \boldsymbol{\omega}_i, \quad \boldsymbol{\Theta}_i|_{t=0} = \boldsymbol{\Theta}_{i,0}. \tag{12}$$

Note that Eq. (12) is completely decoupled from the other equations.

2.2.3. Hydrodynamic interactions

To determine the unknown rigid body motions $(\boldsymbol{U}_i, \boldsymbol{\omega}_i)$ of the particles, one needs balance equations for drag forces and torques on particle boundaries. In the absence of inertia and external forces or torques, particles are force-free and torque-free:

$$\boldsymbol{F}_i = \int_{\partial P_i(t)} \boldsymbol{\sigma} \cdot \boldsymbol{n} \, \mathrm{d}s = 0, \tag{13}$$

$$\boldsymbol{T}_i = \int_{\partial P_i(t)} (\boldsymbol{x} - \boldsymbol{X}_i) \times (\boldsymbol{\sigma} \cdot \boldsymbol{n}) \, \mathrm{d}s = 0, \tag{14}$$

where $\boldsymbol{T}_i = T_i \boldsymbol{k}$ and $\boldsymbol{n}$ is a normal vector on ∂P_i pointing out of the particle. In this study, we do not use any artificial collision schemes which have been commonly used in others' works: e.g. [6].

2.3. The sliding bi-periodic frame constraints

A sliding frame which contains a small number of particles can represent an infinite number of such systems because of the bi-periodicity as described in Fig. 2. Here, we discuss mathematical descriptions of the bi-periodicity in the sliding frame. From Fig. 2, the kinematic relation for the horizontal periodicity between Γ_2 and Γ_4 is obvious:

$$\boldsymbol{u}(0, y) = \boldsymbol{u}(L, y), \quad y \in [0, H], \tag{15}$$

for all t. We also need a condition for the force balance:

$$\boldsymbol{t}(0, y) = -\boldsymbol{t}(L, y), \quad y \in [0, H], \tag{16}$$

where $\boldsymbol{t}$ are tractions on the boundaries.

The vertical sliding periodicity between Γ_1 and Γ_3 is more complicated, since it is time-dependent. One needs to take into account (i) coincidence in positions, (ii) the velocity continuity and (iii) the force balance between Γ_1 and Γ_3, to obtain mathematical conditions for the vertical periodicity. First, let us consider the coincidence in positions between the lower boundary Γ_1 and the upper boundary Γ_3. As shown in Fig. 2, a point a in the frame Ω_A can be identified with point b in the same frame, because point a, viewed from the frame Ω_B, is the same as point b in the frame Ω_A. The difference in the x coordinate locations of the two points is determined by the amount of slide Δ of Eq. (1). If the slide Δ is larger than the width of the domain L (or less than 0), a modular value of Δ with respect to L should be used as the amount of slide inside a bi-periodic frame. Second, consider the continuity in velocity components between two coincident points. The points a and b in frame Ω_A have the same y-directional velocity; however, the x-directional velocity of point

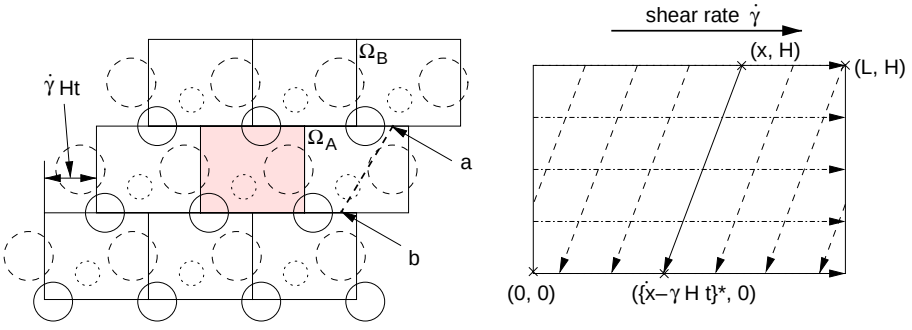

Fig. 2. A three-particle configuration in a sliding bi-periodic domain can represent an infinite number of particles in an unbounded domain of the same configuration (*left*). Kinematic relations for the bi-periodicity in a sliding frame is presented at a certain elapsed time t (*right*).

a is larger than that of point b by the amount of $\dot{\gamma}H$, since frame Ω_B translates faster than Ω_A by this amount. Therefore, the kinematic condition for the sliding periodicity can be written as

$$\boldsymbol{u}(x,H;t) = \boldsymbol{u}(\{x-\dot{\gamma}Ht\}^*,0;t) + \boldsymbol{f}, \quad x \in [0,L). \tag{17}$$

$\boldsymbol{f} = (\dot{\gamma}H, 0)$ originates from the difference in the x-directional velocity component; $\{\cdot\}^*$ denotes a modular function of L: e.g., $\{1.7L\}^* = 0.7L$ and $\{-1.7L\}^* = 0.3L$. Finally, force balances between Γ_1 and Γ_3 can be expressed in terms of traction $\boldsymbol{t}$ in a similar fashion:

$$\boldsymbol{t}(x,H;t) = -\boldsymbol{t}(\{x-\dot{\gamma}Ht\}^*,0;t), \quad x \in [0,L). \tag{18}$$

Eqs. (15)–(18) complete the governing equation set for the fluid domain (with Eqs. (2)–(5)).

In the weak formulation of the finite element method, kinematic constraints are usually combined with Lagrangian multipliers and, as a result, force balances are satisfied implicitly through the multipliers. In this regard, we will use only the kinematic equations (Eqs. (15) and (17)) in the derivation of the weak form in Section 3 and, throughout the study, we call the two equations the sliding bi-periodic frame constraints.

2.4. Boundary-crossing particles

In this section, we consider particles which cross the computational domain boundaries Γ (Fig. 3). In such a situation, particles or parts of a particle which are present outside the computational domain need to be relocated into the domain. In addition, the rigid-body motion of a relocated (part of) particle can be different from that of the original particle. Let us consider the relocation of coordinates. From the rigid-ring description, the relocation involves two consecutive steps: relocation of particle centers and relocation of particle boundaries. The relocation of the particle boundary should be made based on a relocated particle center, if the particle center has been relocated. Both relocations can be described by a single equation. A position $\boldsymbol{x} = (x,y)$, which is present outside the domain, shall belong to one of four regions (upper, lower, left and right regions) as shown in Fig. 3. For a given $(\dot{\gamma},H,t)$, the relocated position $\boldsymbol{x}' = (x',y')$ is determined according to the region to which the original position belongs:

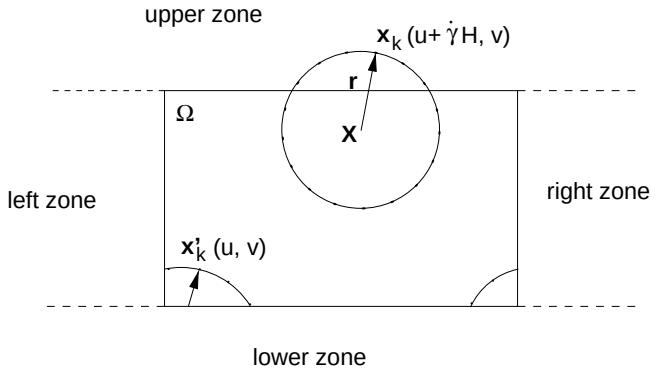

Fig. 3. Description of a particle crossing the domain boundary: The part of a particle which is present outside the domain is relocated according to Eq. (19). If a particle crosses the upper and thereby lower boundaries, the x-directional translational velocities for different parts of the particle are different by the amount of $\dot{\gamma}H$.

$$\begin{aligned}
&\text{upper zone:} \quad (x', y') = (\{x - \dot{\gamma} H t\}^*, y - H),\\
&\text{lower zone:} \quad (x', y') = (\{x + \dot{\gamma} H t\}^*, y + H),\\
&\text{right or left zone:} \quad (x', y') = (\{x\}^*, y),\\
&\text{otherwise:} \quad (x', y') = (x, y),
\end{aligned} \tag{19}$$

where $\boldsymbol{x}$ (and $\boldsymbol{x}'$) can be either a particle center $\boldsymbol{X}$ (and $\boldsymbol{X}'$) or a point on a particle boundary. The y coordinate relocation in Eq. (19) need not involve a modular function, since particles should be smaller than the size of the domain. The last line in Eq. (19) is added for consistency in notation of coordinates on particle boundaries. We keep two sets of coordinates for particle boundaries: the unprimed set is for the original coordinate before relocation and the primed one is for relocated coordinates including particles or parts of particles which are not relocated.

The upper frame translates faster than the computational domain by the amount of $\dot{\gamma} H$ and the lower frame moves slower by $(-\dot{\gamma} H)$. Thus, relocation involves changes in the x-directional translational velocity component U of a particle, when a particle center or parts of a particle cross the upper and (thereby) lower sliding boundaries, or the other way around. Changes in the rigid-body motion can be expressed in a single equation for both a particle center and parts of a particle, which is determined by the region where the original position is located:

$$\begin{aligned}
&\text{upper zone:} \quad U' = U - \dot{\gamma} H,\\
&\text{lower zone:} \quad U' = U + \dot{\gamma} H,\\
&\text{otherwise:} \quad U' = U.
\end{aligned} \tag{20}$$

Again, the last line is added for consistency in notation.

It would be worthwhile to discuss the use of Eqs. (19) and (20) to avoid possible confusion. Relocation of the particle center is used only in the time integration of the kinematic equation (Eq. (11)) for a given configuration of particles, because one can always construct a particle configuration such that all particle centers are present inside the computational domain. So the particle center does not take part in constructing the weak form which will be discussed in the following section. On the other hand, the primed coordinate of the particle boundary is part of the actual computational configuration of particles which should be incorporated in the weak form (Section 3.3.2.).

3. Weak form

We follow the approach of Glowinski et al. [6] in the derivation of the weak form in the sense that fluid–particle interactions are treated implicitly via the combined weak formulation where hydrodynamic force and torque on a particle boundary exactly cancel. However, we will make a few modifications for the rigid-ring description of particles (Eqs. (6)–(10)) and for the sliding bi-periodic frame constraints in Eqs. (15) and (17). We first start with simple systems consisting of non-boundary-crossing particles and extend the weak form to cover boundary-crossing particle systems in the end.

3.1. Combined weak form for the fluid domain

We have only the constraint equations on Γ, rather than explicit boundary conditions. To incorporate this situation with the standard velocity–pressure formulation, we assume that there are specified (unknown) tractions $\boldsymbol{t}$ on Γ, which satisfy the force balance of the sliding bi-periodic frame (Eqs. (16) and (18)). Then, the standard weak formulation leads to an integral term of the traction force along Γ which vanishes,

since the boundary tractions are canceled out mutually according to the force balance equations (Eqs. (16) and (18)).

Let us define the combined solution and variational space for velocity:

$$\mathsf{V} = \{(\boldsymbol{v}, \boldsymbol{V}_1, \ldots, \boldsymbol{V}_N, \boldsymbol{\chi}_1, \ldots, \boldsymbol{\chi}_N) | \boldsymbol{v} \in H^1(\Omega \setminus P(t)),\ \boldsymbol{V}_i \in \Re^2,\ \boldsymbol{\chi}_i = \chi_i \boldsymbol{k} \in \Re,\ \boldsymbol{v} = \boldsymbol{V}_i + \boldsymbol{\chi}_i \times (\boldsymbol{x} - \boldsymbol{X}_i) \text{ on } \partial P_i(t) \text{ (for } i = 1, \ldots, N)\}.$$

The solution space for pressure is $L^2(\Omega \setminus P(t))$. To incorporate constraint equations for the sliding bi-periodic frame (Eqs. (15) and (17)), we introduce two Lagrangian multipliers, $\boldsymbol{\lambda}^{\mathrm{h}} = (\lambda_x^{\mathrm{h}}, \lambda_y^{\mathrm{h}})$ defined on the left boundary (Γ_4) and $\boldsymbol{\lambda}^{\mathrm{v}} = (\lambda_x^{\mathrm{v}}, \lambda_y^{\mathrm{v}})$ on the upper boundary (Γ_3). $\boldsymbol{\lambda}^{\mathrm{h}}$ is for the horizontal periodicity of Eq. (15) and $\boldsymbol{\lambda}^{\mathrm{v}}$ is for the vertical sliding periodicity of Eq. (17). The proper function spaces for the Lagrangian multipliers would be

$$\boldsymbol{\lambda}^{\mathrm{h}} \in L^2(\Gamma_4), \quad \boldsymbol{\lambda}^{\mathrm{v}} \in L^2(\Gamma_3).$$

The choice of Γ_4 rather than Γ_2 (or, Γ_3 rather than Γ_1) is arbitrary, but the sign of a multiplier changes according to the choice. The physical meaning of the two multipliers is the traction force on the sliding frame boundary. Considering a stack of an infinite number of frames (as in Fig. 2), the boundary traction is simply an internal force to attach neighboring frames. The identity between the multipliers and tractions will be discussed in Section 4.

By using (i) the governing equations (Eqs. (2)–(4)) for the fluid domain, (ii) the hydrodynamic force-free torque-free conditions (Eqs. (13) and (14)) and (iii) the constraint equations for the sliding frame boundary (Eqs. (15) and (17)) with the Lagrangian multipliers $\boldsymbol{\lambda}^{\mathrm{h}}$ and $\boldsymbol{\lambda}^{\mathrm{v}}$, one gets the combined weak form for the fluid domain as follows:

Find $(\boldsymbol{u}, \boldsymbol{U}_i, \boldsymbol{\omega}_i) \in \mathsf{V}$, $p \in L^2(\Omega \setminus P(t))$, $\boldsymbol{\lambda}^{\mathrm{h}} \in L^2(\Gamma_4)$, and $\boldsymbol{\lambda}^{\mathrm{v}} \in L^2(\Gamma_3)$ $(i = 1, \ldots, N)$ such that

$$-\int_{\Omega \setminus P(t)} p \nabla \cdot \boldsymbol{v} \, \mathrm{d}A + \int_{\Omega \setminus P(t)} 2\eta \boldsymbol{D}(\boldsymbol{u}) : \boldsymbol{D}(\boldsymbol{v}) \, \mathrm{d}A + \langle (\boldsymbol{\lambda}^{\mathrm{v}}, \boldsymbol{v}(x, H; t) - \boldsymbol{v}(\{x - \dot{\gamma} H t\}^*, 0; t) \rangle_{\Gamma_3} + \langle \boldsymbol{\lambda}^{\mathrm{h}}, \boldsymbol{v}(0, y) - \boldsymbol{v}(L, y) \rangle_{\Gamma_4} = 0, \tag{21}$$

$$\int_{\Omega \setminus P(t)} q \nabla \cdot \boldsymbol{u} \, \mathrm{d}A = 0, \tag{22}$$

$$\langle \boldsymbol{\mu}^{\mathrm{h}}, \boldsymbol{u}(0, y) - \boldsymbol{u}(L, y) \rangle_{\Gamma_4} = 0, \tag{23}$$

$$\langle \boldsymbol{\mu}^{\mathrm{v}}, \boldsymbol{u}(x, H; t) - \boldsymbol{u}(\{x - \dot{\gamma} H t\}^*, 0; t) \rangle_{\Gamma_3} = \langle \boldsymbol{\mu}^{\mathrm{v}}, \boldsymbol{f} \rangle_{\Gamma_3}, \tag{24}$$

for all $(\boldsymbol{v}, \boldsymbol{V}_i, \boldsymbol{\chi}_i) \in \mathsf{V}$, $q \in L^2(\Omega \setminus P(t))$, $\boldsymbol{\mu}^{\mathrm{h}} \in L^2(\Gamma_4)$ and $\boldsymbol{\mu}^{\mathrm{v}} \in L^2(\Gamma_3)$ $(i = 1, \ldots, N)$.

The inner product $\langle \cdot, \cdot \rangle_{\Gamma_j}$ is the standard inner product in $L^2(\Gamma_j)$:

$$\langle \boldsymbol{\mu}, \boldsymbol{v} \rangle_{\Gamma_j} = \int_{\Gamma_j} \boldsymbol{\mu} \cdot \boldsymbol{v} \, \mathrm{d}s.$$

The forcing term $\boldsymbol{f}$ in Eq. (24) originates from the difference in the sliding velocities of the upper and and lower boundaries (Eq. (17)) and it is constant for given $(\dot{\gamma}, H)$.

3.2. Combined weak form for the particle domain

The rigid-ring problem is a fluid problem with rigid-body motions assigned as the boundary condition. Therefore, the corresponding weak form can be obtained in a similar fashion as the fluid domain. Since particles are distinct from one another, we can deal with each particle separately and here we derive the weak form for the ith particle P_i. The solution and variational space for the velocity is

$$\tilde{\mathrm{V}}_i = \{(\boldsymbol{v}, \boldsymbol{V}_i, \boldsymbol{\chi}_i) | \boldsymbol{v} \in H^1(P_i(t)),\ \boldsymbol{V}_i \in \Re^2,\ \boldsymbol{\chi}_i = \chi_i \boldsymbol{k} \in \Re,\ \boldsymbol{v} = \boldsymbol{V}_i + \boldsymbol{\chi}_i \times (\boldsymbol{x} - \boldsymbol{X}_i) \text{ on } \partial P_i(t)\}.$$

The corresponding space for the pressure is $L^2(P_i(t))$. In the rigid-ring problem, the pressure is constant over the particle. By using the governing equations for the particle domain (Eqs. (6)–(8)) and the hydrodynamic equations (Eqs. (13) and (14)), the combined weak form for the particle P_i is given by:Find $(\boldsymbol{u}, \boldsymbol{U}_i, \boldsymbol{\omega}_i) \in \tilde{\mathrm{V}}_i$ and $p \in L^2(P_i(t))$ such that

$$-\int_{P_i(t)} p \nabla \cdot \boldsymbol{v} \, \mathrm{d}A + \int_{P_i(t)} 2\eta \boldsymbol{D}(\boldsymbol{u}) : \boldsymbol{D}(\boldsymbol{v}) \, \mathrm{d}A = 0, \tag{25}$$

$$\int_{P_i(t)} q \nabla \cdot \boldsymbol{u} \, \mathrm{d}A = 0, \tag{26}$$

for all $(\boldsymbol{v}, \boldsymbol{V}_i, \boldsymbol{\chi}_i) \in \tilde{\mathrm{V}}_i$ and $q \in L^2(P_i(t))$.

3.3. Weak form for the whole domain

The weak form for the whole domain can be obtained by using the procedure of Glowinski et al. [6]: (i) extend the combined velocity space to cover the particle domain and (ii) remove the rigid-ring constraint in the combined velocity space by enforcing it as a constraint equation in the weak form. In order to introduce constraint equations on particle boundaries, we need to define another Lagrangian multiplier $\boldsymbol{\lambda}^{p,i} = (\lambda_x^{p,i}, \lambda_y^{p,i})$ on $\partial P_i(t)$. The physical meaning of the multiplier is a traction on the particle boundary, which will be discussed in Section 4.3 in detail. The proper function space is again

$$\boldsymbol{\lambda}^{p,i} \in L^2(\partial P_i(t)).$$

As a result, the weak form for the whole domain can be stated as follows:

Find $\boldsymbol{u} \in H^1(\Omega)^2$, $\boldsymbol{U}_i \in \Re^2$, $\boldsymbol{\omega}_i \in \Re$, $\boldsymbol{\lambda}^{p,i} \in L^2(\partial P_i(t))$, $p \in L^2(\Omega)$, $\boldsymbol{\lambda}^{\mathrm{h}} \in L^2(\Gamma_4)$ and $\boldsymbol{\lambda}^{\mathrm{v}} \in L^2(\Gamma_3)$ $(i = 1, \ldots, N)$ such that

$$\begin{aligned} &-\int_\Omega p \nabla \cdot \boldsymbol{v} \, \mathrm{d}A + \int_\Omega 2\eta \boldsymbol{D}(\boldsymbol{u}) : \boldsymbol{D}(\boldsymbol{v}) \, \mathrm{d}A + \sum_i^N \langle \boldsymbol{\lambda}^{p,i}, \boldsymbol{v} - (\boldsymbol{V}_i + \boldsymbol{\chi}_i \times (\boldsymbol{x} - \boldsymbol{X}_i)) \rangle_{\partial P_i} \\ &\quad + \langle (\boldsymbol{\lambda}^{\mathrm{v}}, \boldsymbol{v}(x, H; t) - \boldsymbol{v}(\{x - \dot{\gamma} H t\}^*, 0; t) \rangle_{\Gamma_3} + \langle \boldsymbol{\lambda}^{\mathrm{h}}, \boldsymbol{v}(0, y) - \boldsymbol{v}(L, y) \rangle_{\Gamma_4} = 0 \end{aligned} \tag{27}$$

$$\int_\Omega q \nabla \cdot \boldsymbol{u} \, \mathrm{d}A = 0, \tag{28}$$

$$\langle \boldsymbol{\mu}^{p,i}, \boldsymbol{u} - (\boldsymbol{U}_i + \boldsymbol{\omega}_i \times (\boldsymbol{x} - \boldsymbol{X}_i)) \rangle_{\partial P_i} = 0 \quad (i = 1, \ldots, N), \tag{29}$$

$$\langle \boldsymbol{\mu}^{\mathrm{h}}, \boldsymbol{u}(0, y) - \boldsymbol{u}(L, y) \rangle_{\Gamma_4} = 0, \tag{30}$$

$$\langle \boldsymbol{\mu}^{\mathrm{v}}, \boldsymbol{u}(x, H; t) - \boldsymbol{u}(\{x - \dot{\gamma} H t\}^*, 0; t) \rangle_{\Gamma_3} = \langle \boldsymbol{\mu}^{\mathrm{v}}, \boldsymbol{f} \rangle_{\Gamma_3}, \tag{31}$$

for all $\boldsymbol{v} \in H^1(\Omega)^2$, $\boldsymbol{V}_i \in \Re^2$, $\boldsymbol{\chi}_i \in \Re$, $q \in L^2(\Omega)$, $\boldsymbol{\mu}^{p,i} \in L^2(\partial P_i(t))$, $\boldsymbol{\mu}^{\mathrm{h}} \in L^2(\Gamma_4)$ and $\boldsymbol{\mu}^{\mathrm{v}} \in L^2(\Gamma_3)$ $(i = 1, \ldots, N)$.

3.3.1. Remarks

(1) Force-free, torque-free rigid-body motions of particles are satisfied in a weak sense through rigid-ring constraints (Eqs. (27) and (29)); and the Lees–Edwards boundary condition is combined with the weak form through the sliding bi-periodic frame constraints (Eqs. (27), (30) and (31)).
(2) Once a particle configuration is given, one can solve Eqs. (27)–(31), to get the solution $(\boldsymbol{u}, p, \boldsymbol{U}_i, \boldsymbol{\omega}_i)$ and all the Lagrangian multipliers, and then determine the next particle configuration, using the kinematic equations (Eqs. (11) and (12)). Initial conditions for $\boldsymbol{u}$, $\boldsymbol{U}_i$ and $\boldsymbol{\omega}_i$ are not necessary, since both fluid and particles are inertialess.
(3) It is necessary to specify a reference velocity at a single point in the fluid domain, since the sliding boundary constraints give only relative difference in velocities of the boundaries. To obtain a simple shear flow in the x-direction, the y component of the reference velocity needs to be specified zero. On the other hand, the choice for the x-directional reference velocity is completely arbitrary. Depending on the choice, the average translational velocity of the computational domain can be faster or slower and, as a result, time-dependent particle configurations become different also. However, relative positions of particles and the relative velocity field over the domain do not change according to this choice. We prefer to specify the zero value at the center of Γ_4. Then, the sliding frame stays stationary but the upper boundary moves at the velocity $\frac{1}{2}\dot{\gamma}H$ and the lower boundary moves at $-\frac{1}{2}\dot{\gamma}H$.
(4) The pressure level should be specified through one of the normal components of the Lagrangian multipliers on Γ to the boundary (i.e., λ_x^{h} or λ_y^{v}), since the Lagrangian multiplier is a traction.

3.3.2. Modification of the weak form for boundary-crossing particles

If a particle crosses the domain boundary, Eqs. (27) and (29) in the weak form need to be modified, because (i) a part of the particle is relocated and (ii) the rigid-body motion of a relocated part possibly changes, as mentioned in Section 2.4. Since the primed set $\boldsymbol{x}'$ (Eq. (19)) are the coordinates of particle boundaries in the computational domain, Eqs. (27) and (29) in the weak form should be calculated based on $\boldsymbol{x}'$. However, the vector $(\boldsymbol{x} - \boldsymbol{X}_i)$, pointing at a position on the particle boundary, should be evaluated by the original coordinate $\boldsymbol{x}$. In addition, the velocity U associated with a position $\boldsymbol{x}'$ on the particle boundary, which is different from the velocity at $\boldsymbol{x}$ for relocation involving upper and lower boundaries, should comply with Eq. (20). As a result, we get the following modified form for Eqs. (27) and (29) for a boundary crossing particle P_i:

$$\langle \boldsymbol{\mu}^{p,i}(\boldsymbol{x}'), \boldsymbol{u}(\boldsymbol{x}') - (\boldsymbol{U}_i + \boldsymbol{\omega}_i \times (\boldsymbol{x} - \boldsymbol{X}_i)) \rangle_{\partial P_i} = \langle \boldsymbol{\mu}^{p,i}(\boldsymbol{x}'), \boldsymbol{f}\,' \rangle_{\partial P_i}, \tag{32}$$

where

$$\boldsymbol{f}\,' = \begin{cases} (-\dot{\gamma}H, 0) & \text{from the upper zone,} \\ (\dot{\gamma}H, 0) & \text{from the lower zone,} \\ (0, 0) & \text{otherwise.} \end{cases}$$

Since $\boldsymbol{f}\,'$ is constant for the given $(\dot{\gamma}, H)$, the corresponding variational term with the multiplier $\boldsymbol{\lambda}^{p,i}$ should not be present in Eq. (27).

4. Bulk stress

4.1. Expressions for bulk stress

The bulk stress is the average stress over the domain and it can be expressed, for a volume V, as the sum of the fluid contribution and the particle contribution [10]:

$$\langle \boldsymbol{\sigma} \rangle = \frac{1}{V} \int_V \boldsymbol{\sigma} \, \mathrm{d}V = \frac{1}{V} \int_{V_\mathrm{f}} \boldsymbol{\sigma} \, \mathrm{d}V + \frac{1}{V} \int_{V_\mathrm{p}} \boldsymbol{\sigma} \, \mathrm{d}V,$$

where $\langle \cdot \rangle$ denotes a volume average quantity in V, V_f is the volume occupied by the fluid and V_p is of the particles. If the fluid is Newtonian and the inertia is neglected, one gets

$$\langle \boldsymbol{\sigma} \rangle = -p' \boldsymbol{I} + 2\eta \langle \boldsymbol{D} \rangle + \frac{1}{V} \int_{\partial V_\mathrm{p}} \boldsymbol{x}\boldsymbol{t} \, \mathrm{d}S, \tag{33}$$

where p' is the averaged pressure contribution from the fluid domain ($(1/V) \int_{V_\mathrm{f}} p \, \mathrm{d}V$) and $\boldsymbol{t}$ is the traction force on the particle surface [11]. One may calculate the bulk stress directly from Eq. (33). However, an alternative expression, which involves an integral along the domain boundary only, is also possible, whenever the traction force is known on ∂V. From the momentum balance equation (Eq. (2)), which is valid in the full domain, we find that

$$\frac{\partial}{\partial x_k} \left(x_i \sigma_{kj} \right) = \sigma_{ij}.$$

Integration of this equation and applying the divergence theorem over the volume V, the bulk stress can be expressed by means of the traction force $\boldsymbol{t}$ on ∂V:

$$\langle \boldsymbol{\sigma} \rangle = \frac{1}{V} \int_{\partial V} \boldsymbol{x}\boldsymbol{t} \, \mathrm{d}S \left(= \frac{1}{A_\mathrm{f}} \int_\Gamma \boldsymbol{x}\boldsymbol{t} \, \mathrm{d}s \right). \tag{34}$$

The expression in the parenthesis is the two-dimensional form for the sliding bi-periodic frame of area A_f.

4.2. Bulk stress by boundary integrals of Lagrangian multipliers

The Lagrangian multipliers $\boldsymbol{\lambda}^\mathrm{h}$ and $\boldsymbol{\lambda}^\mathrm{v}$ for the sliding bi-periodic frame constraints in the weak form (Eqs. (30) and (31)) can be identified by the traction force $\boldsymbol{t}$ on the domain boundary Γ, by comparing the standard weak form under prescribed tractions on Γ with the weak form of the momentum balance (Eq. (27)). Suppose that, for simplicity, there are no boundary-crossing particles, then we find that

$$-\int_\Omega p \nabla \cdot \boldsymbol{v} \, \mathrm{d}A + \int_\Omega 2\eta \boldsymbol{D}(\boldsymbol{u}) : \boldsymbol{D}(\boldsymbol{v}) \, \mathrm{d}A = \int_\Gamma \boldsymbol{t} \cdot \boldsymbol{v} \, \mathrm{d}s,$$

$$-\int_\Omega p \nabla \cdot \boldsymbol{v} \, \mathrm{d}A + \int_\Omega 2\eta \boldsymbol{D}(\boldsymbol{u}) : \boldsymbol{D}(\boldsymbol{v}) \, \mathrm{d}A + (\text{r.b.m.}) = -\int_\Gamma \boldsymbol{\lambda}^{\mathrm{v(or\ h)}} \cdot \boldsymbol{v} \, \mathrm{d}s,$$

where (r.b.m) denotes a collection of particle boundary integrals for rigid-body constraints. Direct comparison of the right-hand side terms gives the following identities between multipliers and tractions:

$$\begin{aligned}
&(t_x(x), t_y(x)) = (\lambda_x^\mathrm{v}(\{x + \dot{\gamma} H t\}^*),\ \lambda_y^\mathrm{v}(\{x + \dot{\gamma} H t\}^*)) \quad \text{on } \Gamma_1, \\
&(t_x(y), t_y(y)) = (\lambda_x^\mathrm{h}(y), \lambda_y^\mathrm{h}(y)) \quad \text{on } \Gamma_2, \\
&(t_x(x), t_y(x)) = (-\lambda_x^\mathrm{v}(x), -\lambda_y^\mathrm{v}(x)) \quad \text{on } \Gamma_3, \\
&(t_x(y), t_y(y)) = (-\lambda_x^\mathrm{h}(y), -\lambda_y^\mathrm{h}(y)) \quad \text{on } \Gamma_4.
\end{aligned} \tag{35}$$

Combining the bulk stress expression by tractions (Eq. (34)) with Eq. (35), the bulk stress over the computational domain can be expressed by boundary integrals of the Lagrangian multipliers along Γ:

$$\langle\sigma_{11}\rangle = \frac{1}{A_f}\int_0^L \left(\{x-\dot{\gamma}Ht\}^* - x\right)\lambda_x^v(x)\,dx + \frac{1}{H}\int_0^H \lambda_x^h(y)\,dy, \tag{36a}$$

$$\langle\sigma_{22}\rangle = -\frac{1}{L}\int_0^L \lambda_y^v(x)\,dx, \tag{36b}$$

$$\langle\sigma_{12}\rangle = \frac{1}{A_f}\int_0^L \left(\{x-\dot{\gamma}Ht\}^* - x\right)\lambda_y^v(x)\,dx + \frac{1}{H}\int_0^H \lambda_y^h(y)\,dy = -\frac{1}{L}\int_0^L \lambda_x^v(x)\,dx. \tag{36c}$$

We have two expressions in Eq. (36c); one is from $\langle\sigma_{12}\rangle$ and the other from $\langle\sigma_{21}\rangle$, which give the same result. In derivation of Eqs. (36a)–(36c), we used the following integral identity along the sliding boundary:

$$\int_0^L x\lambda_x^v(\{x+\dot{\gamma}Ht\}^*)\,dx = \int_0^L \left(\{x-\dot{\gamma}Ht\}^*\right)\lambda_x^v(x)\,dx.$$

4.3. Bulk stress for systems containing boundary-crossing particles

Let us extend the bulk stress expression in Eqs. (36a)–(36c) to cover systems containing particles crossing the domain boundaries. First, consider the physical meaning of the Lagrangian multipliers $\boldsymbol{\lambda}^p$ on the boundary of the particle which is completely immersed in the computational domain. (For a moment, we omit the index i for simplicity.) Comparing the weak form of the momentum balance (Eq. (27)), the bulk stress expression of Eq. (33), and the expression by the Lagrangian multipliers (Eqs. (36a)–(36c)), the particle contribution to the bulk stress in Eq. (33) can be replaced by integral of $\boldsymbol{\lambda}^p$:

$$\int_{\partial P} \boldsymbol{x}\boldsymbol{\lambda}^p\,ds = \int_{\partial P} \boldsymbol{x}\boldsymbol{t}\,ds + pV_p\boldsymbol{I}. \tag{37}$$

That is, the multiplier $\boldsymbol{\lambda}^p$ is the traction force $\boldsymbol{t}$ exerted by the fluid on the particle boundary, including the fictitious pressure p inside the rigid ring, which is a constant. Though Eq. (37) cannot be used for a boundary-crossing particle, the relation of the multiplier $\boldsymbol{\lambda}^p$ to the traction force is the same for such a case.

Now consider the system containing particles crossing the computational domain. First notice that, in such a case, the left-hand-side integral of Eq. (37) does not represent the stress contribution from the particle with the relocated particle boundary coordinate $\boldsymbol{x}'$, since the relocated coordinate does not form a complete circle. The integral of Eq. (37) should be evaluated with the original coordinate $\boldsymbol{x}$ for the particle boundary. However, care should be exercised in the interpretation of the particle contribution to the bulk stress evaluated with the original coordinate, because parts of the particle described by $\boldsymbol{x}$ are located outside the computational domain. Consider an infinite number of sliding bi-periodic domains. Suppose that every domain has the same configuration of particles because of the bi-periodicity and that a finite number of particles are crossing the domain boundary. Now, let us take the average of the bulk stresses over all the domains into account. Then, the error in the averaged bulk stress caused by the stress contribution of particles crossing the boundary, converges to zero, since the number of these boundary particles scales with the size of the boundary, whereas the total number of particles scales with the volume. Therefore, if there is a particle crossing the domain boundary, the stress contribution from the particles can be obtained by replacing the relocated coordinate $\boldsymbol{x}'$ by the original coordinate $\boldsymbol{x}$ (but still keeping the traction force from the relocated coordinate $\boldsymbol{\lambda}^p(\boldsymbol{x}')$) in Eq. (37). Therefore, for N_c particles crossing the boundary, the bulk stress expression can be achieved by replacing the particle contribution with the relocated coordinate by that of the original coordinate as follows:

$$\langle \boldsymbol{\sigma}' \rangle = \langle \boldsymbol{\sigma} \rangle + \frac{1}{A_{\mathrm{f}}} \sum_{k=1}^{N_{\mathrm{c}}} \int_{\partial P_k} (\boldsymbol{x} - \boldsymbol{x}') \boldsymbol{\lambda}^{p,k}(\boldsymbol{x}') \, \mathrm{d}s, \tag{38}$$

where $\langle \boldsymbol{\sigma} \rangle$ is the result of the boundary integrals in Eqs. (36a)–(36c). If all particles are completely immersed in the domain, then $\boldsymbol{x}' = \boldsymbol{x}$ and Eq. (38) becomes identical to Eqs. (36a)–(36c). Eqs. (36) and (38) complete the expression of bulk stress for general particle configuration in the bi-periodic sliding frame. We have two remarks:

(1) In derivation of Eqs. (36) and (38), we only use the identity relation of the Lagrangian multipliers $(\boldsymbol{\lambda}^{\mathrm{h(or\ v)}}, \boldsymbol{\lambda}^{\mathrm{p}})$ with boundary tractions so that Eqs. (36) and (38) are not restricted to a Newtonian fluid.
(2) Eqs. (36a)–(36c) consists of only boundary integrals along Γ, which is much more efficient than evaluating the bulk stress by volume integrals and particle boundary integrals. Also, for the evaluation of the boundary integrals along Γ, the coefficients for numerical integration can be taken from the discretized global matrix equation, since the boundary integrals are already present in the weak form (Eqs. (27)–(31)).

5. Implementation

5.1. Spatial discretizations

5.1.1. Discretization of computational domain

Two discretization schemes have been used in the simulations of particulate flows in combination with fictitious-domain finite-element methods. A regular finite element triangulation for the velocity and a twice-coarser triangulation for the pressure were used by Glowinski et al. [6], whereas Yu et al. [8] employed a rectangular discretization with the bilinear velocity and constant pressure interpolations (Q_1–P_0), to avoid asymmetry in triangulations which possibly leads to non-symmetric drift of particles. However, their Q_1–P_0 element does not satisfy the so-called inf–sup condition. In this study, we use a regular rectangular discretization again but with the bi-quadratic interpolation of the velocity and the linear discontinuous interpolation for the pressure, so-called Q_2–P_1^{d} element (Fig. 4), which satisfies the inf–sup condition. A discontinuous interpolation of the pressure appears to be mandatory, since an arbitrary location of a particle boundary induces discontinuity in the pressure across the boundary. Baaijens [9] illustrated erroneous results associated with continuous interpolations of the pressure in a fluid–structure interaction problem with a fictitious domain method, which has discontinuity in pressures across a solid boundary.

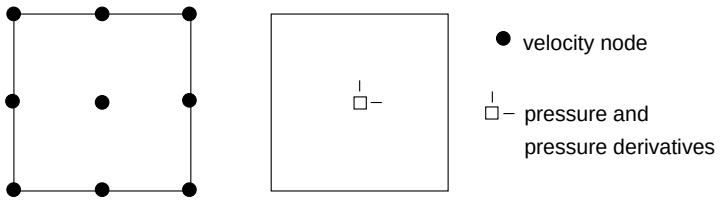

Fig. 4. The Q_2–P_1^{d} element with the bi-quadratic interpolation for the velocity and the linear discontinuous interpolation for the pressure.

5.1.2. Implementation of rigid-ring constraint

From the rigid-ring description, we discretize particles by their boundaries. In this study, the weak form of the rigid-ring description (Eq. (32)) has been approximated by point collocation:

$$\langle \boldsymbol{\mu}^{p,i}(\boldsymbol{x}'), \boldsymbol{u}(\boldsymbol{x}') - (\boldsymbol{U}_i + \boldsymbol{\omega}_i \times (\boldsymbol{x} - \boldsymbol{X}_i)) \rangle_{\partial P_i} \approx \sum_{k=1}^{M^i} \boldsymbol{\mu}_k^{p,i} \cdot \{ \boldsymbol{u}(\boldsymbol{x}'_k) - (\boldsymbol{U}_i + \boldsymbol{\omega}_i \times (\boldsymbol{x}_k - \boldsymbol{X}_i)) \}, \tag{39}$$

where M^i, $\boldsymbol{x}_k$, $\boldsymbol{x}'_k$ and $\boldsymbol{\mu}_k^{p,i}$ are the number of collocation points on ∂P_i, the original coordinate of the kth collocation point, the relocated coordinate of the kth collocation point and the collocated multiplier $\boldsymbol{\mu}^{p,i}$ at $\boldsymbol{x}'_k$, respectively. An obvious reason for a choice of the point collocation is its simplicity in implementation especially for boundary-crossing particles. Implementation of Eq. (39) with relocated collocation points circumvents tedious boundary integrals over the splitted particle boundary.

We define equally distributed collocation points on a particle boundary (based on the original coordinate) and the number of collocation points M^i is proportional to the radius of a particle. Too large number of M^i causes element-locking, while too small number of M^i cannot represent the rigid-body motion of a circular particle accurately. Approximately one collocation point in an element appears to give the most accurate result, as we will see in Section 6. A small change in M^i, say 10%, from the optimal number does not affect solutions (velocities, pressures, rigid-body motions of particles and values of Lagrangian multipliers) much, but this gives an additional control to avoid particle collisions, although it hardly occurs in our simulation with a reasonable time step size.

5.1.3. Implementation of sliding bi-periodic constraints

Let us consider the constraint equation in the weak form for horizontal periodicity (Eq. (30)), which involves a boundary integral of $\boldsymbol{\mu}^{\mathrm{h}}$ along Γ_4 with velocities on Γ_4 and Γ_2. Because of the regular discretization of the computational domain, the facing elements between Γ_4 and Γ_2 are always conforming. In such a case, the collocation at all nodes appears to be the best method which produces the most accurate solution, since a rearrangement of the matrix equation, by eliminating $\boldsymbol{\lambda}^{\mathrm{h}}$ by row and column manipulations, gives the matrix equation of the physically connected mesh system. The nodal collocation can be expressed as follows:

$$\langle \boldsymbol{\mu}^{\mathrm{h}}, \boldsymbol{u}(0,y) - \boldsymbol{u}(L,y) \rangle_{\Gamma_4} \approx \sum_{i=1}^{\mathrm{NND}_4} \boldsymbol{\mu}_i^{\mathrm{h}} \cdot (\boldsymbol{u}(0,y_i) - \boldsymbol{u}(L,y_i)), \tag{40}$$

where NND_4 is the number of all nodes (including the first and the last nodes) on Γ_4 (or Γ_2).

Now, let us consider the implementation of the vertical sliding periodicity. We rewrite the boundary integral term in the left-hand side of Eq. (31) for convenience:

$$\int_0^L \boldsymbol{\mu}^{\mathrm{v}}(x) \cdot \Big(\boldsymbol{u}(x,H;t) - \boldsymbol{u}(\{x - \dot{\gamma} H t\}^*, 0; t) \Big) \, \mathrm{d}x. \tag{41}$$

The second integral in Eq. (41) involves an integral over facing element boundaries attached on Γ_3 and Γ_1. As illustrated in Fig. 5, the connection of the facing elements are non-conforming and time-dependent. This situation is analogous to the mortar-finite element contact description in frictional contact surface problems in solid mechanics, where the traction and kinematic compatibility are approximated across non-conforming interfaces [12]. In those problems, it has been known that optimal convergence rates are only obtained when integral representations of contact constraints based on mortar element methods are utilized, rather than methods based on nodal collocations. There are several choices for interpolations of the multiplier space of $\boldsymbol{\mu}^{\mathrm{v}}$: linear/quadratic or continuous/discontinuous interpolations. Seshayer and Suri [13]

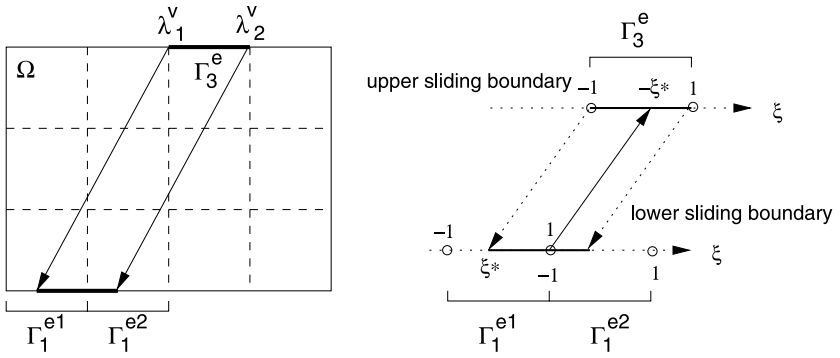

Fig. 5. Non-conforming facing elements for sliding periodicity between the upper and lower domain boundaries at a certain elapsed time (*left*); and the exact sliding boundary integral by splitting the range of integral (*right*).

reported that the use of uniform continuous interpolation of the multiplier, one order lower than the interpolation of the primary variable (in this case, velocity), gives a good convergence in such a problem.

To solve the vertical sliding boundary constraint equation in combination with integral representations of $\boldsymbol{\mu}^{\mathrm{v}}$ by Gaussian quadrature, the second integral in Eq. (41) should be splitted into two sub integrals based on the lower facing elements. Fig. 5 describes this situation with a linear continuous interpolation of $\boldsymbol{\mu}^{\mathrm{v}}$ at a certain elapsed time. An element boundary denoted by Γ_3^e on Γ_3 is attached over two boundary elements on Γ_1, $\Gamma_1^{e_1}$ and $\Gamma_1^{e_2}$. Suppose a local coordinate system with $\xi \in [-1,1]$ for each element boundary. If the left corner node of Γ_3^e corresponds to the local coordinate ξ^* on $\Gamma_1^{e_1}$, then the node between the two lower boundary elements will be connected to the local coordinate $(-\xi^*)$ in Γ_3^e. Now an element boundary integral of the second term in Eq. (41) can be written as a sum of two sub integrals:

$$\begin{aligned}&\int_{\Gamma_3^{e_3}} \boldsymbol{\mu}^{\mathrm{v}}(x)\cdot\boldsymbol{u}(\{x-\dot{\gamma}Ht\}^*,0;t)\,\mathrm{d}x\\ &\quad=\int_{-1}^{-\xi^*}\boldsymbol{\mu}^{\mathrm{v}}(\xi)\cdot\boldsymbol{u}_{\Gamma_1^{e_1}}(\xi;\xi^*)\left|\frac{\mathrm{d}x}{\mathrm{d}\xi}\right|\mathrm{d}\xi+\int_{-\xi^*}^{1}\boldsymbol{\mu}^{\mathrm{v}}(\xi)\cdot\boldsymbol{u}_{\Gamma_1^{e_2}}(\xi;\xi^*)\left|\frac{\mathrm{d}x}{\mathrm{d}\xi}\right|\mathrm{d}\xi,\end{aligned}\tag{42}$$

which can be solved exactly by Gaussian quadrature after rescaling. In Eq. (42), $\boldsymbol{u}_{\Gamma_1^{e_1}}$ and $\boldsymbol{u}_{\Gamma_1^{e_2}}$ are interpolated velocities on element boundaries $\Gamma_1^{e_1}$ and $\Gamma_1^{e_2}$, respectively. In Section 6.1, we compare performances of several mortar element interpolations for the vertical sliding constraint equation to choose the best interpolation of the multiplier space. In addition erroneous results will be illustrated, which are caused by integrals without considering the splitting intervals in the element boundary in Eq. (42).

5.1.4. Matrix equation

Using the discretizations mentioned above, one gets the following matrix equation at each time step for a given particle configuration:

$$\begin{bmatrix} K & G & 0 & P & H & V\\ G^{\mathrm{T}} & 0 & 0 & 0 & 0 & 0\\ 0 & 0 & 0 & R & 0 & 0\\ P^{\mathrm{T}} & 0 & R^{\mathrm{T}} & 0 & 0 & 0\\ H^{\mathrm{T}} & 0 & 0 & 0 & 0 & 0\\ V^{\mathrm{T}} & 0 & 0 & 0 & 0 & 0 \end{bmatrix}\begin{pmatrix} \boldsymbol{u}\\ \tilde{p}\\ \tilde{\boldsymbol{U}}\\ \boldsymbol{\lambda}^{\mathrm{p}}\\ \boldsymbol{\lambda}^{\mathrm{h}}\\ \boldsymbol{\lambda}^{\mathrm{v}} \end{pmatrix}=\begin{bmatrix} 0\\ 0\\ 0\\ \tilde{\boldsymbol{f}}'\\ 0\\ \tilde{\boldsymbol{f}} \end{bmatrix},\tag{43}$$

where $\tilde{p}$, $\tilde{\boldsymbol{U}}$, $\tilde{\boldsymbol{f}}$, and $\tilde{\boldsymbol{f}}'$ are pressure variables, rigid-body motion variables, the forcing term due to the vertical sliding periodicity (Eq. (31)), and integral of the forcing term due to boundary-crossing particle (Eq. (32)). This symmetric sparse matrix is solved by a direct method based on a sparse multifrontal variant of Gaussian elimination (HSL/MA41) [14–16].

5.2. Time integration

For a given particle configuration, if necessary after relocation, one can construct and solve the matrix equation in Eq. (43) and then rigid-body motions of particles are obtained as a part of the solution. Particle positions for the next time step are obtained by integrating the kinematic equation for each particle (Eq. (11)). We employ explicit time integration schemes; the explicit Euler method at the first time step and the second-order Adams–Bashforth method from the second time step. However, a modification of the original scheme is necessary for the Adams–Bashforth method to comply with the sliding bi-periodic frame concept when particles cross the (upper and lower) domain boundaries. The second-order Adams–Bashforth needs the present particle position, the previous particle velocity, and the present particle velocity. When the present particle center has come from outside of the upper or lower frame boundary via relocation (Eq. (19)), one has to modify the previous velocity according to changes in the x-directional translational velocity of the particle (Eq. (20)). (The next particle position should be evaluated based on the present relocated particle position and the present velocity.) Therefore, we get the following modification in the second-order Adams–Bashforth scheme for the particle P_i, which has come from the upper or lower boundary, in the x-direction:

$$X_i^{n+1} \approx X_i'^{n} + \Delta t\left(\tfrac{3}{2}U_i^n - \tfrac{1}{2}U_i'^{n-1}\right), \tag{44}$$

where $X_i'^{n}$, X_i^{n+1}, U_i^n and $U_i'^{n-1}$ are the present (relocated) particle position, the next particle position, the present velocity and the modified previous velocity, respectively. The modified previous velocity $U_i'^{n-1}$ is determined by Eq. (20) in Section 2.4. This modification can be extended to higher-order explicit integral schemes, by keeping updating previous velocities of a particle.

6. Verification

6.1. Performance of sliding boundary integral by mortar elements

Here, we discuss the performance of several mortar element techniques for the sliding periodic constraint discussed in Section 5.1.3 and illustrate the necessity of the exact sliding boundary integral of Eq. (42). We tested five schemes: (i) nodal collocation, (ii) an integral method with continuous linear interpolation of the multiplier space in combination with the exact sliding boundary integral, (iii) continuous quadratic interpolation with the exact sliding boundary integral and (iv, v) inexact integrals by two- or three-point Gaussian quadrature with continuous linear interpolation (not using splitted interval as in Eq. (42). The test problem is a single particle of radius 0.1 freely suspended at the center of the sliding bi-periodic domain of size 1×1 with $\dot{\gamma} = 1$ and $\eta = 1$. In this choice, the amount of slide $\Delta = \dot{\gamma}Ht$ is simply represented by the elapsed time t and the problem is time-periodic with period $T = 1$. We used a rather coarse mesh, 20×20, to amplify numerical discrepancies, and the number of collocation points on the particle boundary is chosen to be 12. The velocity at the center of the boundary Γ_4 has been specified to be zero. As a result, the particle does not translate, but rotates at a periodic angular velocity $\omega(t)$, which is determined by the relative configuration of the sliding bi-periodic frames.

Plotted in Fig. 6(a) are periodic variations of $\omega(t)$ implemented with different mortar element methods. The nodal collocation and the inexact integrals with two- and three-point Gaussian quadrature produce exact values only at special time steps when the elements on Γ_1 and Γ_3 are conforming. The continuous linear and quadratic interpolations with the splitting integral of Eq. (42) give satisfactory angular velocities for all time steps, regardless of the element conformity. Next, let us investigate the distribution of the Lagrangian multiplier along the sliding boundary. The accurate evaluation of the Lagrangian multipliers is of great importance in our simulation, since the bulk stress is calculated from the multipliers as explained in Section 4. Fig. 6(b) shows distributions of the multiplier λ_x^v along Γ_3 at a certain elapsed time $t = 0.06$, when the elements to be connected are not conforming. Both the inexact integrals show discrepancy near the two corners (at $x = 0$ and 1) and the quadratic interpolation gives a singular result. Only the linear interpolation in combination with the exact sliding integral appears to be satisfactory, which is consistent with the results of Seshaijer and Suri [13]. From now on, we use the linear continuous interpolation with the exact sliding boundary integral for all simulations in this work.

6.2. Verification

In this section we verify our formulation and numerical schemes through a simple example problem. To the best knowledge of the authors, there is neither an analytic solution nor a previous numerical result on particulate flows in a sliding bi-periodic frame of Lees–Edwards. Therefore, we will make a comparison between our regular mesh problem and a corresponding boundary-fitted mesh problem. However, solution techniques for boundary-fitted mesh problems are not straight forward either, because of (i) sliding bi-periodic constraints and (ii) force-free torque-free rigid-body motions of particles. In order to resolve the problem (i), we made a restriction to a special time step, $t = 0$ (initial). If a finite element mesh of the boundary-fitted problem is constructed such that the element conformity is satisfied in both horizontal and vertical directions, then simple nodal collocation techniques in both directions give correct solutions at $t = 0$ under the sliding bi-periodic frame constraints. Problem (ii) can be resolved by decomposing the

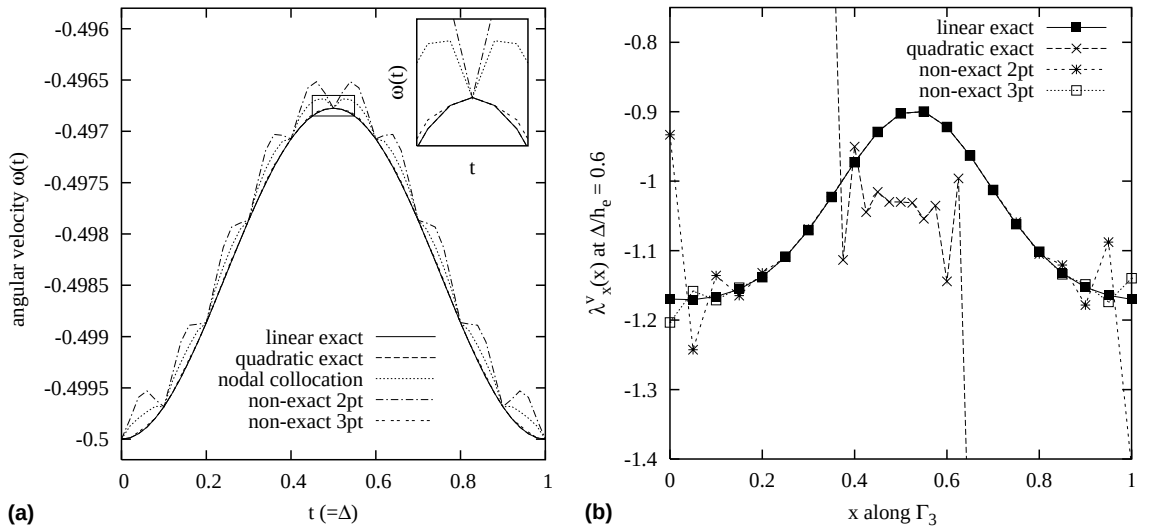

Fig. 6. Comparison of several mortar element techniques for the sliding boundary integral: (a) angular velocity of the particle for $t \in [0, 1]$ and (b) distribution of the Lagrangian multiplier λ_x^v along Γ_3 when $t = 0.06$.

original problem into several subproblems and by applying superposition of the solutions from the subproblems to satisfy the force-free and torque-free conditions on the particle boundary.

A system containing two symmetrically located particles is selected as a test problem: two particles of the same radius 0.15 are freely suspended in a sliding bi-periodic frame of size 1×1 with $\eta = 1$ and $\dot{\gamma} = 1$. We use three regular meshes consisting of 25-by-25, 50-by-50 and 100-by-100 elements, which are denoted by M1, M2 and M3, respectively. The number of collocation points for a single particle is 26 for M1, 52 for M2 and 104 for M3. There are (approximately) one, two and four elements between the two particles for M1, M2 and M3, respectively. The boundary fitted mesh has about 45-by-45 elements and there are 16 elements between the two particles. Fig. 7 shows the mesh M1 and the boundary-fitted mesh. We intentionally plotted a twice coarser mesh for the boundary-fitted one for clarity. As mentioned, the boundary-fitted mesh is constructed to attain mesh conformity between the facing boundaries in both directions. So, for the boundary-fitted problem, the sliding bi-periodic constraints are implemented by nodal collocation in both directions; the rigid-body motion problem is treated by superposition. We performed mesh refinement to get convergent solutions for the boundary-fitted problem also.

Table 1 lists the rigid-body solution of the upper left particle. The coarse mesh M1 leads to about 2% relative error compared to the boundary-fitted solution and, for the fine mesh M3, the error becomes 0.05%. In Figs. 8–10, we present comparison results for the velocity, the pressure and the velocity gradient, respectively, along the two diagonals: the diagonal (/) without crossing particles (continuous phase) and the diagonal (\) crossing the particles (discontinuous phase). The accuracy of our regular mesh solution along the discontinuous line is expected to be worse. Plotted in Fig. 8 is the fluctuation velocity u_f, the total velocity subtracted by the given simple shear velocity, $u - \dot{\gamma}(y - 0.5)$. Along the continuous diagonal, all three regular meshes give satisfactory results over the whole range (Fig. 8(a)). Solutions along the discontinuous diagonal (Fig. 8(b)) are found satisfactory also and they show uniform convergence as mesh refinement. Even the coarse M1 mesh, which has a single element between the particles, gives an almost exact velocity there. Next, let us look at pressure comparison results in Fig. 9. Pressure distributions of all three meshes along the continuous diagonal are satisfactory over the whole range and show uniform convergence with mesh refinement. A small discrepancy can be observed between the particles for the coarse meshes M1 and M2, which have only one and two elements there. Pressures are discontinuous along

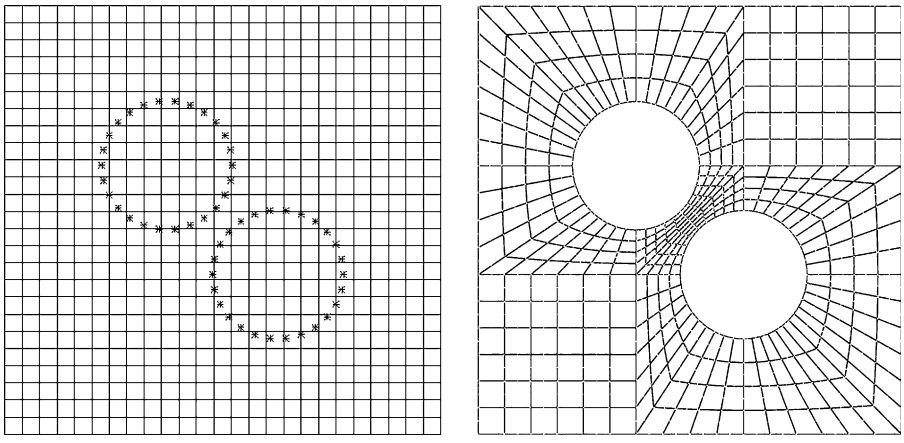

Fig. 7. A regular 25-by-25 (M1) finite element mesh (*left*) and a boundary-fitted mesh, twice coarser than the actual mesh used in comparison (*right*). The coordinates of the particle centers are (p_1, p_2) and (p_2, p_1): $p_1 = 0.18\cos(0.75\pi) + 0.5$; $p_2 = 0.18\sin(0.75\pi) + 0.5$.

Table 1
The mesh refinement result of rigid-body solutions of the left upper particle

Mesh	U	V	ω	Error
M1 (25×25)	0.0789386	0.0481223	−0.504601	2.20419×10^{-2}
M2 (50×50)	0.0791094	0.0481699	−0.5	1.16857×10^{-2}
M3 (100×100)	0.0794421	0.0478371	−0.5	5.39294×10^{-4}
Boundary-fitted	0.0794582	0.0478210	−0.5	–

The error is defined by $|(U - U_{bf})/U_{bf}| + |(V - V_{bf})/V_{bf}| + |(\omega - \omega_{bf})/\omega_{bf}|$, where the subscript 'bf' indicates the solution of the boundary-fitted problem.

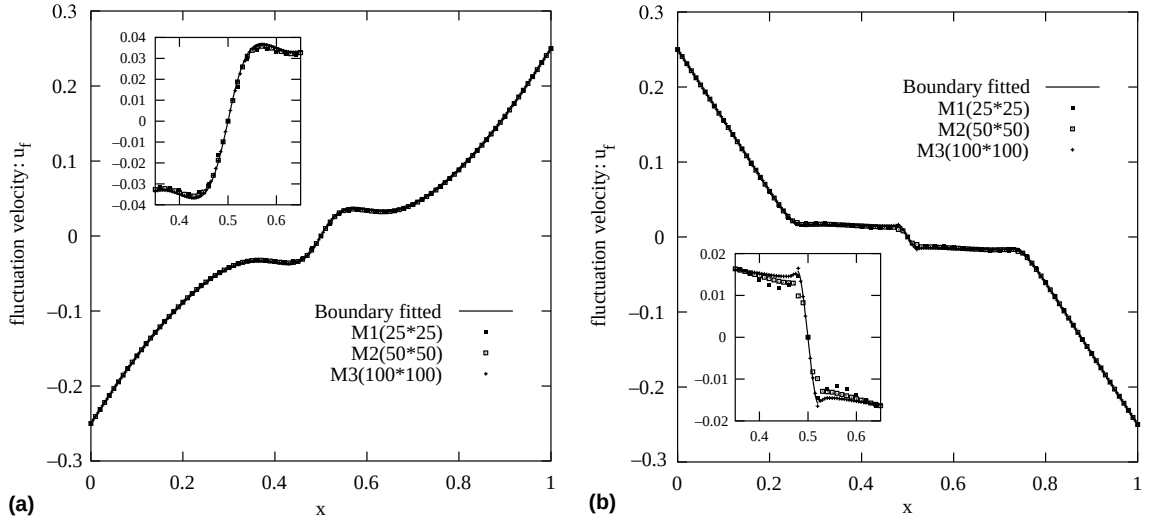

Fig. 8. Comparison of the fluctuation velocity u_f: (a) along the diagonal (/) without crossing particles and (b) along the diagonal (\) crossing the particles. The fluctuation velocity is defined as $u_f(x, y) = u(x, y) - \dot{\gamma}(y - 0.5)$.

the discontinuous diagonal and they show uniform convergence to the boundary-fitted result (Fig. 9(b)). The error caused by the relatively small number of elements between the particles is small. Finally we made a comparison for the velocity gradient by using $(II_{2\boldsymbol{D}})^{1/2}$, where $II_{2\boldsymbol{D}}$ is the second invariant of $2\boldsymbol{D}$. The results, plotted in Fig. 10, show uniform convergence and they are almost exact even along the discontinuous diagonal.

As mentioned earlier, we do not need an artificial particle–particle collision scheme, possibly because we use a fully implicit scheme in determining the particle rigid-body motion. Although collisions hardly occur in our simulations, a rather large time step to accelerate computations possibly causes collisions. In those cases, we use about 10% more points than the most accurate number of collocation points, in order to avoid collision. Here we show the effect of the number of collocation points. Plotted in Fig. 11 are the relative errors in the rigid-body solution of the upper left particle compared with the boundary-fitted results, as a function of the number of collocation points. Mesh M3 is used as a test mesh and the most accurate solutions were produced with 104 points. As indicated, the error due to a 10% increase (or decrease) of the number of collocation points is less than 0.5% in the rigid-body motion.

Finally, we notice that we tested the performance of the numerical scheme when particles cross the upper and lower boundary of the domain. For that we used a problem similar to the two particle case we will

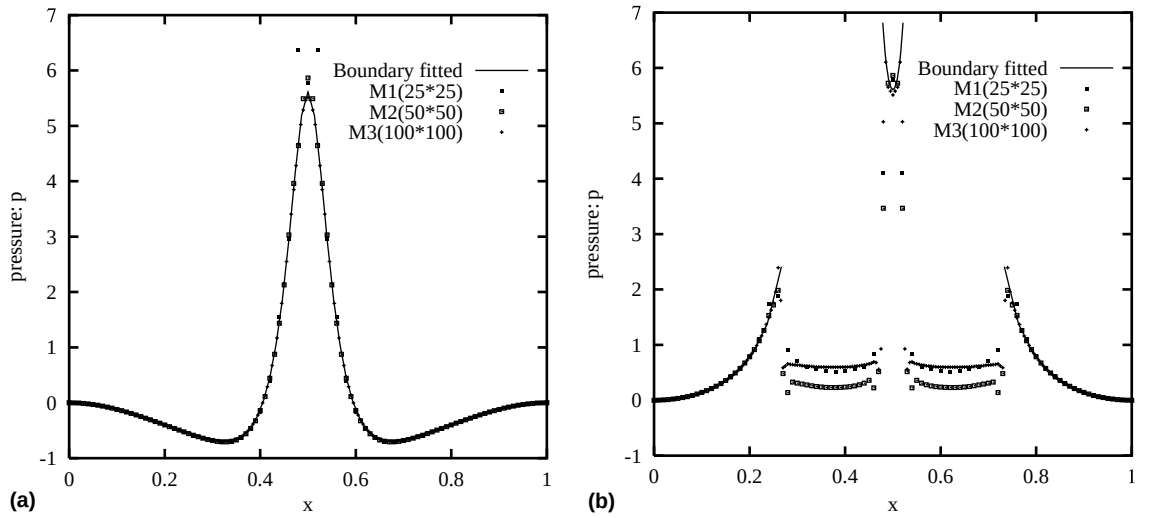

Fig. 9. Comparison of the pressure: (a) along the diagonal (/) without crossing particles and (b) along the diagonal (\) crossing the particles.

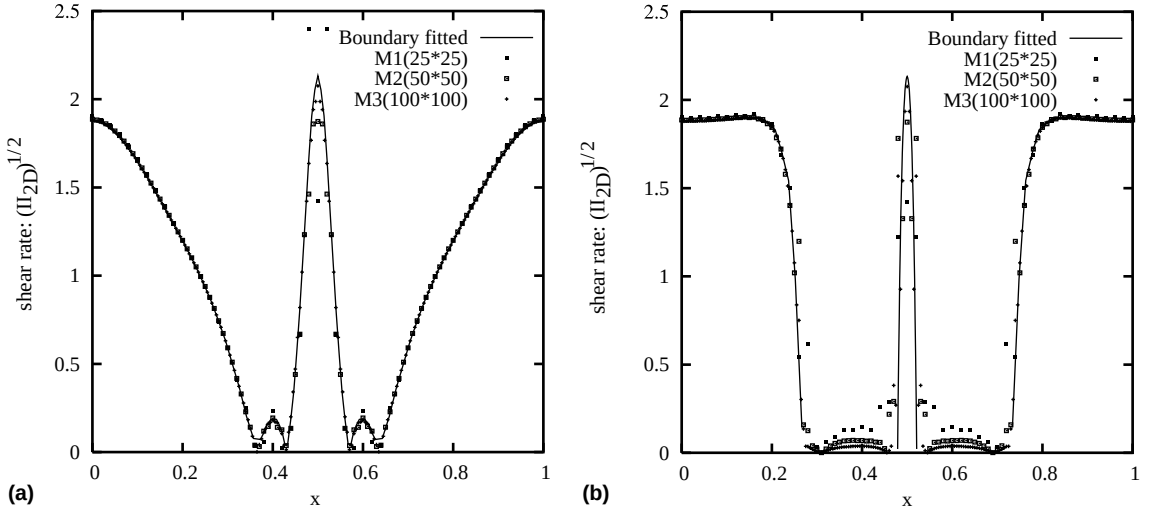

Fig. 10. Comparison of the total shear rate: (a) along the diagonal (/) without crossing particles and (b) along the diagonal (\) crossing the particles. The total shear rate is defined by the second invariant of $2\boldsymbol{D}$, i.e., $(II_{2\boldsymbol{D}})^{1/2}$.

discuss in Section 7.2, however, now with two particles in the center of the cell and two particles crossing the upper and lower boundaries. We verified that in this symmetrically located four particle problem the relative movement of the two particles in the center are the same as the two particles crossing the boundary. We also verified that by shifting the 'window' such that all four particles are fully inside the square domain, the bulk stress as a function of time remains the same. Since this four particle problem does not give any more physical information as the two particle problem in Section 7.2, we have not included any data here.

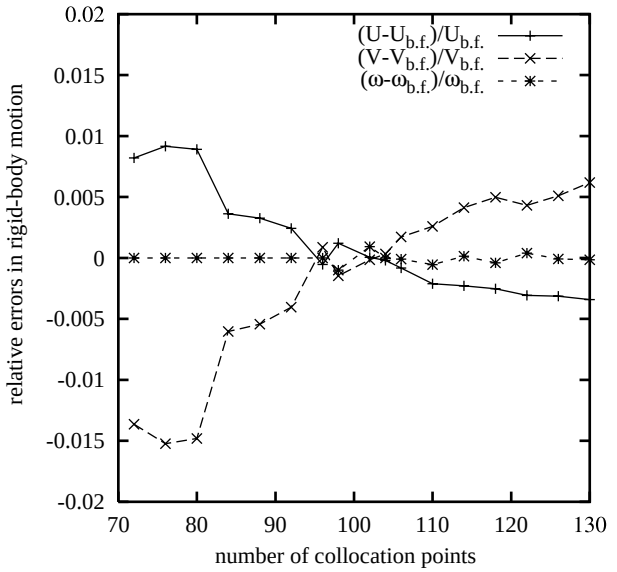

Fig. 11. Relative errors in the rigid-body solution of the left upper particle with increment of the number of collocation points on the particle boundary.

7. Example problems

In this section we present three example problems to demonstrate the feasibility of our formulation and numerical schemes: a single particle, two particles and six particles in a sliding bi-periodic frame. Because of the bi-periodicity in the computational domain, a few particle system in a single domain can be extended to a problem with an infinite number of particles in a unbounded domain.

7.1. Single particle

The first test problem is stated as follows: a single particle of radius r is suspended freely at a center of a sliding bi-periodic domain of size 1×1 under a given shear rate $\dot{\gamma} = 1$ in a Newtonian fluid of the viscosity $\eta = 1$. The reference velocity has been specified at the center of the left domain boundary Γ_4 so that the upper and lower boundaries translate at velocities '$1/2\dot{\gamma}$' and '$-(1/2)\dot{\gamma}$', respectively. As a result, the particle does not translate relatively to the frame, but rotates at the angular velocity $\omega(t)$ which is time-periodic with period $T = L/\dot{\gamma}H = 1$. This problem represents a regular configuration of an infinite number of such a particle system as described in Fig. 12. The initial configuration is reproduced after the time period T. We used a 50-by-50 (or 100-by-100 for very small or very large r) mesh for this problem with 52 (or corresp. 104) collocation points, which were found to give the most accurate solution in Section 6.2.

Plotted in Fig. 13 is the angular velocity of the particle as a function of time for various values of the radius r. The angular velocity fluctuates with respect to t as mentioned, according to the relative configuration of sliding frames. The magnitude of the angular velocity becomes maximum when the distance between particles is minimum (and vice versa) and the fluctuation amplitude increases with the particle radius. Using the boundary integral expressions in Eqs. (36a)–(36c), the time-dependent bulk shear and normal stresses have been calculated and they are plotted in Fig. 14. The bulk shear stress $\langle\sigma_{12}\rangle$ is always larger than '1', which is the contribution from the Newtonian medium. The bulk shear stress becomes maximum when the distance between particles is minimum. The bulk shear stress grows at increasing rate

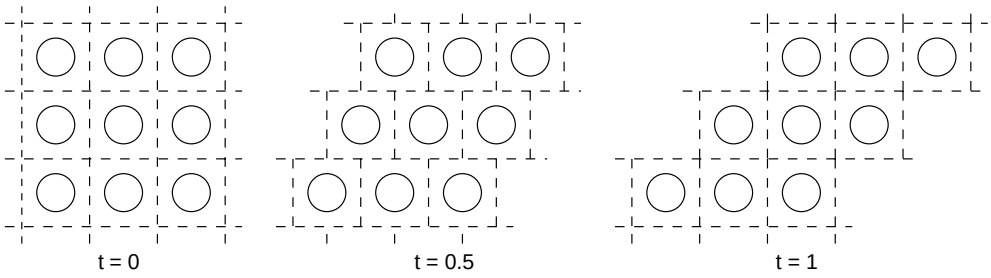

Fig. 12. The single-particle problem in a sliding bi-periodic frame represents a regular configuration of an infinite number of particle systems. The initial configuration is reproduced after time period $T = L/\dot{\gamma}H = 1$.

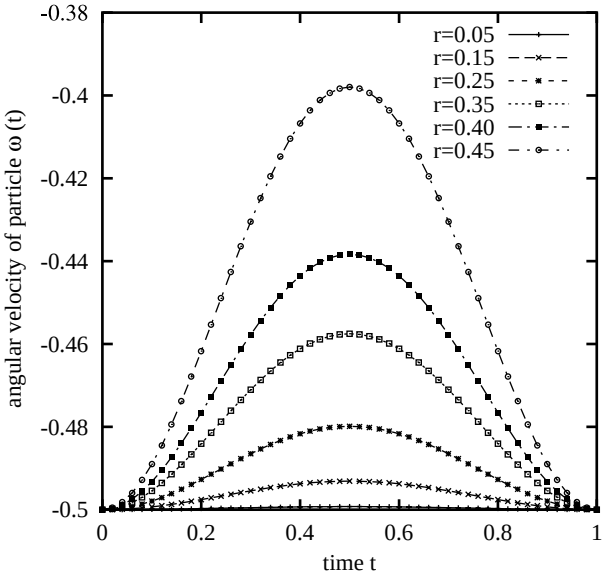

Fig. 13. The angular velocity fluctuation of the single particle problem.

with the particle radius. The bulk normal stress $\langle N_1 \rangle$, defined by $\langle \sigma_{11} - \sigma_{22} \rangle$, again fluctuates periodically according to the configuration of frames at a period T. It becomes zero when the distance between particles is either maximum or minimum. The magnitude of the bulk normal stress is comparable to that of the bulk shear stress of the same particle radius. However, the time average of the bulk normal stress is zero, which means that particles do not contribute to the normal stress in the average sense of the single particle problem.

By taking the time average of bulk shear stresses for a period T, we get the bulk shear viscosity denoted by $\langle \eta \rangle$ which also grows at increasing rate with the solid area fraction ϕ. Einstein's classical result for a dilute suspension with circular disk particles is given by $\langle \eta \rangle = \eta(1 + 2\phi)$ [17]. We performed numerical simulations over a wide range of the area fraction ϕ: from extremely low area fraction (less than 1%) to extremely high fraction (about 75%). The maximum solid area fraction $\phi_{\max}$ for the single particle problem is $\pi/4$. The bulk shear viscosity is plotted with respect to ϕ in Fig. 15.

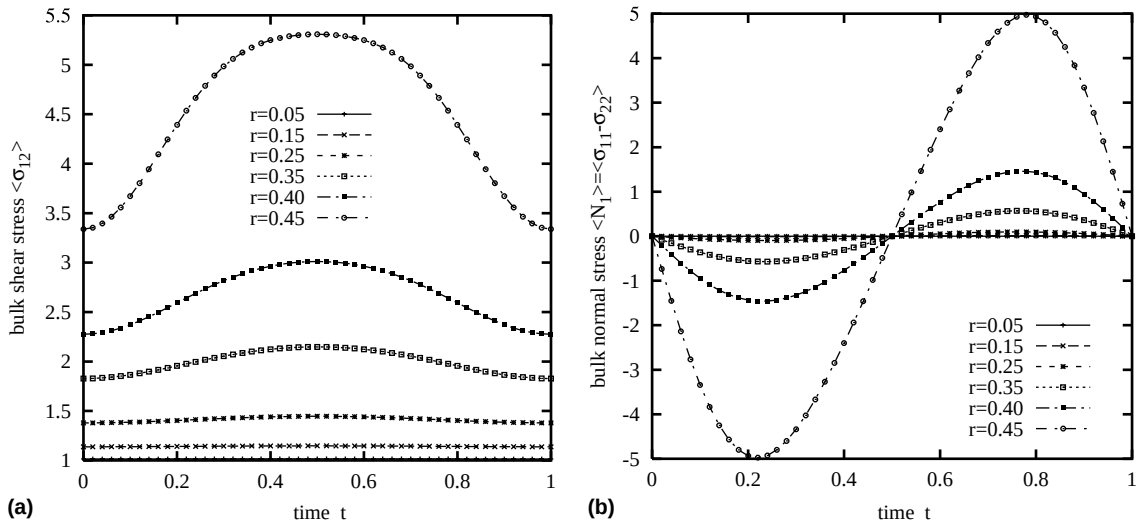

Fig. 14. The bulk shear and normal stresses of the single-particle problem.

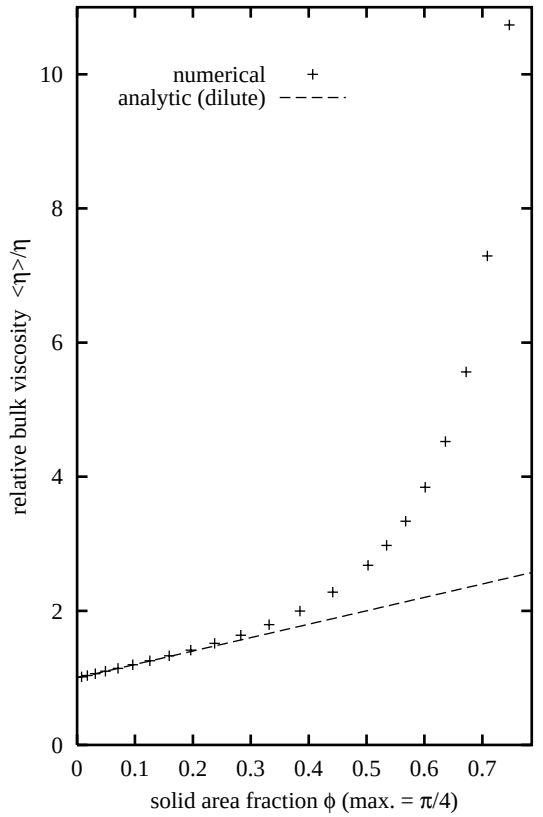

Fig. 15. Time-averaged bulk shear viscosity as a function of solid area fraction ϕ. (Calculated from the single particle problem.)

7.2. Two particles

The second problem is constructed to investigate effects of hydrodynamic interactions between two particles and is stated as follows: two identical particles of radius r are suspended freely in a sliding bi-periodic domain of size 1×1 with $\dot{\gamma} = 1$ and $\eta = 1$. Denoting the left upper particle by P_1 and the right lower one by P_2 (Fig. 16), initial locations of the particles are chosen symmetrically such that $X_1 = 0.25$ and $X_2 = 0.75$ and that the distance between a particle center and the horizontal centerline of the domain becomes D. The parameter D can be regarded as the strength of hydrodynamic interaction between two particles. Again, the velocity at the center of Γ_4 is specified to be zero. As a result, P_1 moves toward the right, while P_2 moves toward the left. Let us consider two extreme results of the sliding bi-periodicity: (i) When the parameter $D = 0$, the particles do not translate but stay stationary; (ii) When $D = 0.25$, P_1 (P_2) moves in the positive (negative) x-direction and its orbit becomes just a straight line parallel to the shear flow. The value D can be selected between zero and 0.25, since a configuration with D larger than 0.25, say $D = 0.25 + \alpha$ ($0 \leqslant \alpha \leqslant 0.25$), is identical to the configuration with $(D = 0.25 - \alpha)$ because of the sliding bi-periodicity (Fig. 16). Now let us consider symmetry in particle paths. The path of P_1 is completely symmetric with respect to that of P_2 with respect to the domain center $(0.5, 0.5)$. This symmetry still holds after P_1 (P_2) crosses the right (left) domain boundary. However, it does not mean that the path of each particle is symmetric by itself, since the sliding bi-periodicity of the frame has its own time period ($T = 1$) and, in general, the periodicity of the frame is not commensurate with the periodicity in the particle motion. In other words, the motion of particles in the sliding bi-periodic frame is not time-periodic, thereby all the solutions (including velocity, pressure and bulk stress) are not time-periodic either.

We selected the radius of the particle $r = 0.12$ and used a 75-by-75 mesh for the domain; and 64 collocation points are used for each particle. We used 11 different values for the parameter $D : 0, 0.025, 0.05, \ldots, 0.225$ and 0.25. Fig. 17 shows consecutive particle movements in case of $D = 0.025$ as an example. Orbits of the particle centers are plotted in Fig. 18 for all D used here. As mentioned, the particle paths are not periodic on account of incommensurability in motions between the sliding frame and the particles. However, some paths form nearly periodic orbits especially for small D cases where the average distance between particles is large in the frame of interest and from the upper or lower sliding frames: i.e., they are relatively less affected by the incommensurability. In addition, the time T required for returning the original x position of a particle depends strongly on D: $T = 31.21$ for $D = 0.025$ and $T = 3.98$

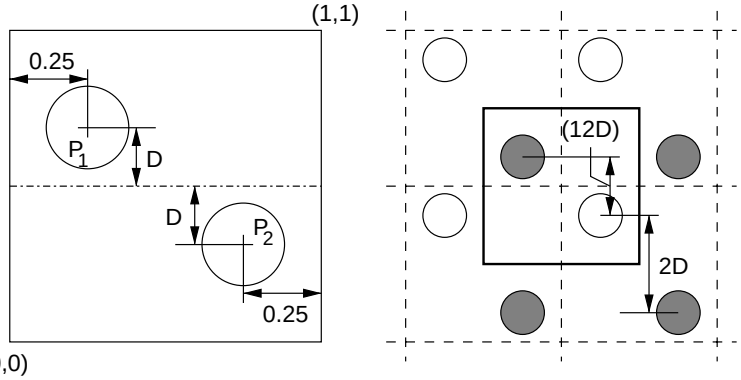

Fig. 16. Initial configuration of the two particle problem (*left*). A configuration with D larger than 0.25 can be represented by the identical configuration with D smaller than 0.25 because of the sliding bi-periodicity (*right*). The dashed line denotes boundaries of the original sliding frames and the bold solid line represent the identical sliding frame.

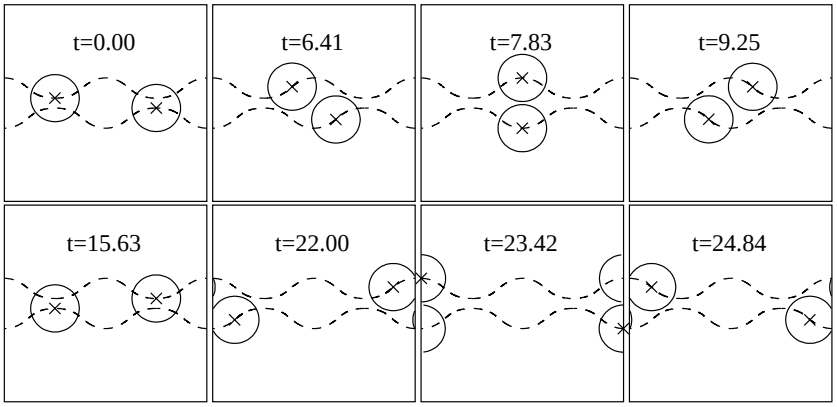

Fig. 17. Time-dependent particle movement in the two particle problem ($D = 0.025$, $r = 0.12$). The dashed curves indicate orbits of the particle centers.

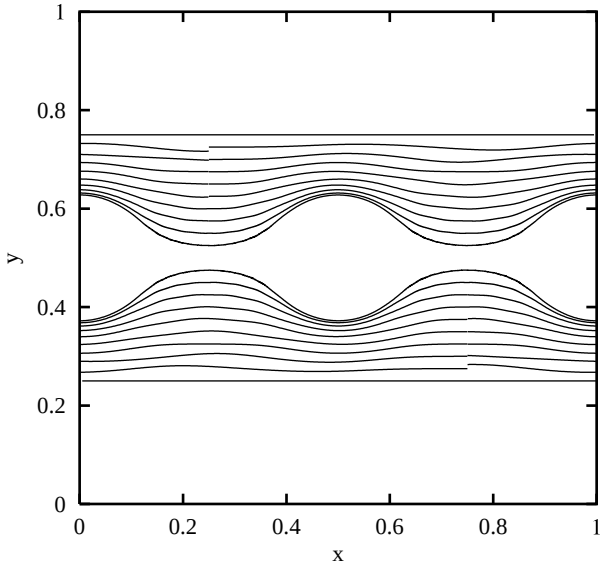

Fig. 18. The orbits of the particle centers in the two particle problem for varying D. The innermost orbit is from $D = 0.025$ and the outermost one (straight line) is from $D = 0.25$. The orbits are not periodic in general.

for $D = 0.25$. (So we will plot numerical results with respect to the x coordinate of the particle P_1 center, $X_1(t)$, which is the same as $(1 - X_2(t))$.)

Plotted in Fig. 19 are the time-dependent bulk shear and normal stresses for $D = 0.025$ and 0.25. As the parameter D increases, the bulk stress curve gradually changes from the curves of $D = 0.025$ to those of 0.25. The bulk shear stress is always larger than '1'. It goes to the maximum value before and after particle contact and becomes minimum when two particles are aligned normal to the shear direction and when they are located far apart. The bulk normal stress fluctuates around the zero line and the time-averaged contribution of the particle to the bulk normal stress is close to zero. Again, the fluctuation amplitude of the bulk normal stress is the same order as that of the bulk shear stress.

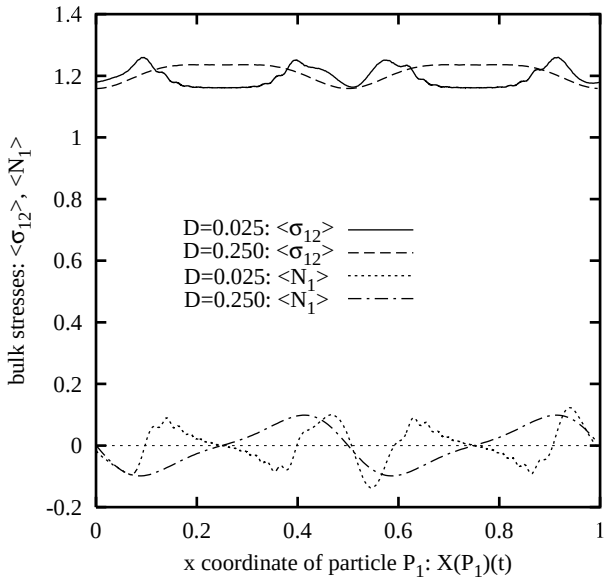

Fig. 19. Time-dependent bulk stresses for $D = 0.025$ and 0.25, with respect to the x coordinate of the particle P_1.

The time-averaged bulk shear viscosity for $r = 0.12$ and for $r = 0.1$ is plotted as a function of D in Fig. 20, after taking the average over a single period. (A straight line in Fig. 20 is the time-averaged bulk shear viscosity for the corresponding single particle problem of the same solid area fraction.) A small dimple near $D = 0.2$ is due to the non-periodicity in the particle orbits of the two particle problem. As indicated in Fig. 20, the bulk shear viscosity increases with D, which seems a bit contradictory to the

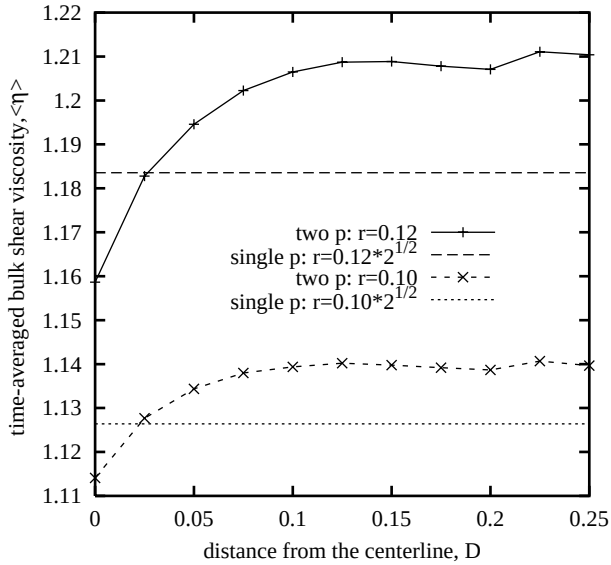

Fig. 20. Time-averaged bulk shear viscosity as a function of D. The average has been taken over a single period.

common understanding: the more interaction of particles, the more viscosity. This result can be interpreted as follows: Let us consider an infinite number of sliding bi-periodic frames of the same particle configuration. As D becomes larger, the average distances between particles in one frame and those in the other decrease. It means that, from the global view point, averaged hydrodynamic interaction increase with increasing D for $D \in (0, 0.25)$. The bulk viscosity for $D \in (0.25, 0.5)$ is obtained from Fig. 20 by using the symmetry: $\langle \eta \rangle_{D=0.25+\alpha} = \langle \eta \rangle_{D=0.25-\alpha}$ for $0 \leqslant \alpha \leqslant 0.25$.

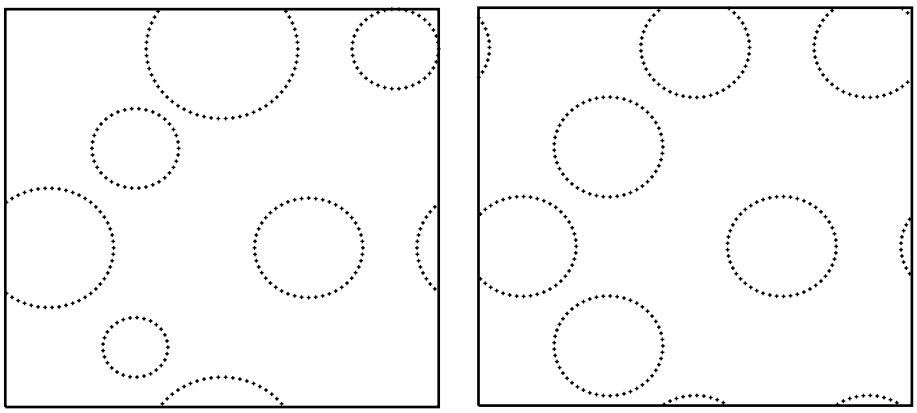

Fig. 21. Initial particle configurations for the six-particle problem: Randomly distributed six particles of different radii (*left*) and six particles of the same radius (*right*). Both have the same solid area fraction $\phi \approx 0.2965$. Particles are described by collocation points.

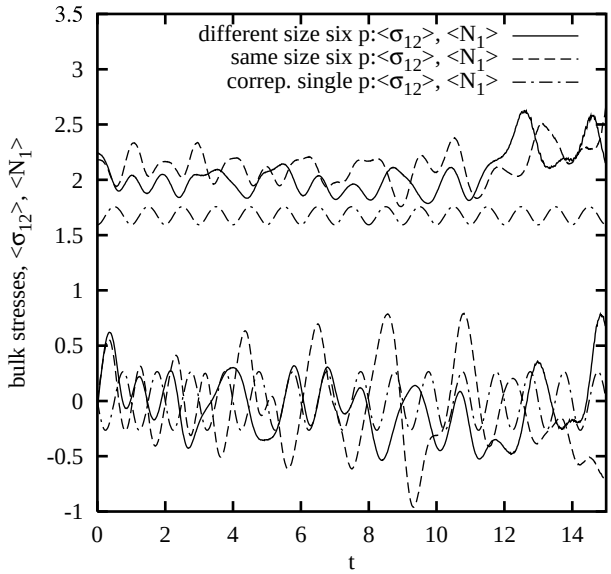

Fig. 22. Bulk normal and shear stress of the six-particle problems. The results are compared with the corresponding single-particle problem with the same solid area fraction.

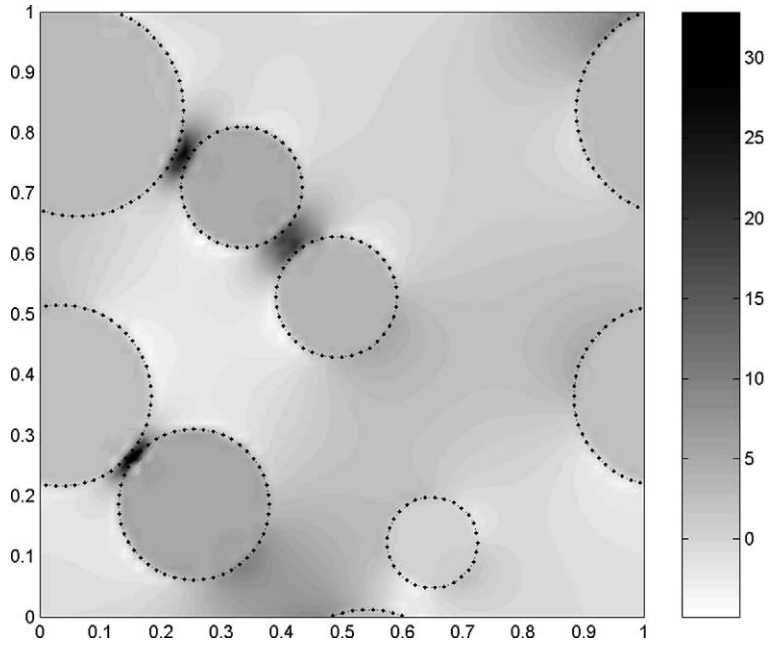

Fig. 23. Pressure distribution at $t = 12.52$ when the bulk shear stress goes to the maximum value in Fig. 22, for the different particle-size case of the six-particle problem.

7.3. Many particles

Now we proceed to more particle problems. We solve two problem sets: one containing equal-sized particles and the other different-sized particles. Both have the same solid area fraction ϕ. Again the problems are defined in a sliding bi-periodic frame of size 1×1 with $\dot{\gamma} = 1$ and $\eta = 1$. Six particles are distributed randomly: for the different particle-size problem, radii of particles are 0.075, 0.1($\times$2), 0.125, 0.1, 0.15 and 0.175; and, for the equal particle-size problem, the radius of particles is about 0.1254. The solid area fraction is approximately 0.2965. We used a 50-by-50 mesh for the computational domain and the number of collocation points are scaled with the particle radius. The computation has been performed for $t = 15$ with a time step equal to 0.01. The initial particle configurations are presented in Fig. 21 and particles are described by their collocation points used in the computation. The bulk stresses for the two problems are plotted in Fig. 22 as a function of t along with the results for the corresponding single particle problem of $r \approx 0.3072$. The observation can be summarized as follows: (i) Bulk shear stresses of the two six-particle problems are always larger than the corresponding single particle result with the same solid area fraction, which shows the effect of increased hydrodynamic interaction; (ii) the particle size distribution does not produce any noticeable changes in the bulk suspension properties; (iii) the bulk normal stresses fluctuate around the zero value for all three cases. In Fig. 23, we plotted the pressure distribution of the different particle-size problem at $t = 12.52$ when the bulk shear stress goes to the maximum value.

8. Conclusions

In this study, a new finite-element formulation for direct simulation of particle suspensions has been developed and implemented. Main features of our formulation can be summarized as follows:

- the sliding bi-periodic frame concept of Lees and Edwards for discrete particles has been extended to continuous fields and combined with the velocity–pressure formulation of the fictitious-domain/finite-element method;
- inertialess particles are described by their boundaries only, eliminating domain discretization of particles, which allows general treatments of boundary-crossing particles;
- a general expression of the bulk stress is derived, which involves only boundary integrals of the Lagrangian multipliers on the domain boundary and on the particle boundary.

The computational domain is discretized regularly with bi-quadratic interpolation of the velocity and linear discontinuous interpolation of the pressure. The sliding bi-periodic constraints are implemented by nodal collocations for the flow direction and by the mortar element technique for the direction normal to the flow. The linear continuous interpolation of the Lagrangian multiplier space appeared to be the best choice for the implementation of the mortar element method. By comparison with the boundary-fitted mesh problem, the accuracy and the convergence of the present scheme have been verified for velocity, pressure and velocity gradient. To demonstrate the feasibility of our scheme, we presented three numerical example problems in two dimensions of single-, two- and six-particle systems in a sliding bi-periodic frame, which represents an infinite number of such configurations in unbounded domain. Through the example problems, we discussed bulk suspension properties together with effects of the solid area fraction and hydrodynamic interactions. The present scheme can be applied to three-dimensional problems without any significant modification and can be extended to suspension problems in viscoelastic fluids in a relatively easy way.

Acknowledgements

This work was supported by the Dutch Polymer Institute. The authors thank Prof. Frank P.T. Baaijens for pointing out the similarity between sliding boundaries and contact problems, which led to the mortar element implementation.

References

[1] B.A.G. Schrauwen, L.E. Govaert, G.W.M. Peters, H.E.H. Meijer, The influence of flow-induced crystallization on the impact toughness of high-density polyethylene, Macromol. Symp. 185 (2002) 89.
[2] A.W. Lees, S.F. Edwards, The computer study of transport processes under extreme conditions, J. Phys. C 5 (1972) 1921.
[3] A.J. Wagner, I. Pagonabarraga, Lees–Edwards boundary conditions for Lattice Boltzmann, J. Stat. Phys. 107 (2002) 521.
[4] A. Lamura, G. Gonnella, Lattice Boltzmann simulations of segregating binary fluid mixtures in shear flow, Physica A (2001) 295.
[5] X.F. Yuan, M. Doi, A general approach for modelling complex fluids: its application to concentrated emulsions under shear, Colloids Surf. A 144 (1998) 305.
[6] R. Glowinski, T.-W. Pan, T.I. Hesla, D.D. Joseph, A distributed Lagrangian multiplier/fictitious domain method for particulate flows, Int. J. Multiphase Flows 25 (1999) 755.
[7] N.A. Patankar, P. Singh, D.D. Joseph, R. Glowinski, T.-W. Pan, A new formulation of the distributed Lagrangian multipliers/fictitious domain method for particulate flows, Int. J. Multiphase Flow 26 (2000) 1509.
[8] Z. Yu, N. Phan-Thien, Y. Fan, R.I. Tanner, Viscoelastic mobility problem of a system of particles, J. Non-Newtonian Fluid Mech. 104 (2002) 87.
[9] F.P.T. Baaijens, A fictitious domain/mortar element method for fluid–structure interaction, Int. J. Numer. Meth. Fluids 35 (2001) 743.
[10] G.K. Batchelor, The stress system in a suspension of force-free particles, J. Fluid Mech. 41 (1970) 545.
[11] N. Phan-Thien, Understanding Viscoelasticity, Springer, Berlin, 2002.
[12] T.A. Laursen, Computational Contact and Impact Mechanics, Springer, Heidelberg, 2002.
[13] P. Seshaijer, M. Suri, hp submeshing via non-conforming finite element methods, Comput. Methods Appl. Mech. Engrg. 189 (2000) 1011.

[14] P.R. Amestoy, I.S. Duff, Vectorization of a multiprocessor multifrontal code, Int. J. Supercomput. Appl. 3 (1989) 41.
[15] P.R. Amestoy, I.S. Duff, Memory management issues in sparse multifrontal methods on multiprocessors, Int. J. Supercomput. Appl. 7 (1989) 64.
[16] P.R. Amestoy, C. Puglisi, An unsymmetrized multifrontal LU factorization, SIAM J. Matrix Anal. Appl. 24 (2002) 553.
[17] J.F. Brady, The Einstein viscosity correction in *n* dimensions, Int. J. Multiphase Flow 10 (1984) 113.